

Experimental constraints on self-consistent reionization models

T. Roy Choudhury[★] and A. Ferrara[★]

SISSA/ISAS, via Beirut 2-4, 34014 Trieste, Italy

Accepted 2005 May 6. Received 2005 April 1; in original form 2004 November 3

ABSTRACT

A self-consistent formalism to jointly study cosmic reionization and thermal history of the intergalactic medium (IGM) in a Λ CDM cosmology is presented. The model implements most of the relevant physics governing these processes, such as the inhomogeneous IGM density distribution, three different classes of ionizing photon sources [massive Population III (PopIII) stars, Population II (PopII) stars and quasi-stellar objects (QSOs)], and radiative feedback inhibiting star formation in low-mass galaxies. By constraining the model free parameters with available data on redshift evolution of Lyman-limit absorption systems, Gunn–Peterson and electron scattering optical depths, near-infrared background and cosmic star formation history, we select a fiducial model, whose main predictions are as follows.

(i) Hydrogen was completely reionized at $z \approx 15$, while He II must have been reionized by $z \approx 12$, allowing for the uncertainties in the ionizing photon efficiencies of stars. At $z \approx 7$, He III suffered an almost complete recombination as a result of the extinction of PopIII stars, as required by the interpretation of the NIRB.

(ii) A QSO-induced complete He II reionization occurs at $z = 3.5$; a similar double H reionization does not take place due to the large number of photons with energies > 13.6 eV from PopII stars and QSOs, even after all PopIII stars have disappeared.

(iii) Following reionization, the temperature of the IGM corresponding to the mean gas density, T_0 , is boosted to 1.5×10^4 K; following that it decreases with a relatively flat trend. Observations of T_0 are consistent with the fact that He is singly ionized at $z \gtrsim 3.5$, while they are consistent with He being doubly ionized at $z \lesssim 3.5$. This might be interpreted as a signature of (second) He II reionization.

(iv) Only 0.3 per cent of the stars produced by $z = 2$ need to be PopIII stars in order to achieve the first hydrogen reionization.

In addition, we get useful constraints on the ionizing photon efficiencies (which are a combination of the star-forming efficiency and the escape fraction of ionizing photons from collapsed haloes) of PopII and PopIII stars, namely, $\epsilon_{\text{PopII}} < 0.01$, $0.002 < \epsilon_{\text{PopIII}} < 0.03$. Varying the efficiencies in these two ranges does not affect the scenario described above. Such a model not only relieves the tension between the Gunn–Peterson optical depth and *WMAP* observations, but also accounts self-consistently for all known observational constraints. We discuss how the results compare with recent numerical reionization studies and other theoretical arguments.

Key words: intergalactic medium – cosmology: theory – large-scale structure of Universe.

1 INTRODUCTION

The study of cosmic reionization has witnessed a very strong advance in the last few years (for a recent review see Ciardi & Ferrara 2005), thanks both to the availability of QSOs located at redshifts $\gtrsim 6$, which allow to probe the physical state of the neutral part of the

intergalactic medium (IGM) via absorption line experiments (Fan et al. 2000, 2001, 2002, 2003), and to the determination of the Thomson electron scattering optical depth τ_{el} from the first-year *WMAP* data (Spergel et al. 2003). A considerable tension from these two data sets has arisen concerning the epoch of hydrogen reionization. In brief, while the rapid increase in the (Gunn–Peterson) $\text{Ly}\alpha$ opacity at $z \gtrsim 5$ could be interpreted, to a first analysis, as an indication of a reionization occurring at $z \approx 6$, the large inferred values of τ_{el} would imply a reionization epoch at $z > 10$. In this regard, one has to

[★]E-mail: chou@sissa.it (TRC); ferrara@sissa.it (AF)

recall that: (i) the first-year *WMAP* result has large error bars; (ii) the limits on τ_{el} depend on the exact analysis technique employed; and (iii) the robustness of the result needs to be confirmed using more data. While on the other hand: (i) the Gunn–Peterson test is very sensitive to even tiny amounts of neutral hydrogen, resulting only in a lower limit to the neutral hydrogen fraction, $x_{\text{HI}} \gtrsim 0.1$ per cent (White et al. 2003); (ii) the experiment has been carried out on a handful of QSOs above $z = 5$ and therefore its statistical significance has still to be evaluated; and (iii) the abrupt increase might be in part due to an incorrect conversion of $\text{Ly}\beta$ to $\text{Ly}\alpha$ optical depths (Songaila 2004). Nevertheless, reasons for the apparent discrepancy must be considered seriously.

A crucial issue about reionization is that this process is tightly coupled to the properties and evolution of star-forming galaxies and QSOs. Hence, the first requirement that any reionization model should fulfill is that it should be able to reproduce the available constraints concerning the luminous sources. Whereas a relatively solid consensus has been reached on the luminosity function, spectra and evolutionary properties of intermediate redshift QSOs, some debate remains on the presence of yet undetected low-luminosity QSOs powered by intermediate mass black holes at high redshift (Ricotti & Ostriker 2004b). The evolution of stellar radiation is instead much less certain. Models corroborated by the observation of an excess in the near-infrared background (NIRB) in the wavelength range 1–4 μm (Magliocchetti, Salvaterra & Ferrara 2003; Salvaterra & Ferrara 2003; Cooray et al. 2004; Kashlinsky et al. 2004) require that the first, metal-free [Population III (PopIII)] stars were very massive if they are to account for this otherwise unexplained excess. The same data require that a quite rapid transition from PopIII to ‘normal’ Population II (PopII) stars must have occurred at about $z = 9$, probably driven by an increase of the metallicity in the active cosmic star formation sites above the critical value $Z_{\text{crit}} = 10^{-5\pm 1} Z_{\odot}$ (Schneider et al. 2002, 2003). Even after that, predicting the joint reionization and star formation histories self-consistently is not an easy task as mechanical and radiative feedback processes can alter the hierarchical structure formation sequence of the underlying dark matter distribution as far as baryonic matter is concerned.

Hence our present aim is to build up self-consistent models that can reconcile the discrepancy between the Gunn–Peterson optical depth and the first-year *WMAP* observations, and at the same time satisfy a larger number of experimental requirements concerning the IGM temperature evolution, He reionization, the number of Lyman-limit systems, the NIRB excess interpretation and the cosmic star formation history. Although this might seem at first sight a very ambitious aim, it turns out that once the relevant physics is included, these results allow a very clear scenario to emerge.

Nothing comes for free, unfortunately, and there is a price to pay for this wealth of predictions that can be obtained via a relatively simple, although physically rigorous, semi-analytical approach to this problem. When compared with the numerical simulations, we can treat many details of the reionization process only in an approximate manner (the shape of ionized region around sources and their overlapping, just to mention a few) and in terms of global averages (such as the filling factor and the clumping factor of ionized regions). However, we have to recall that in order to exploit the full power of the observational data available to constrain models, one must be able to connect widely differing spatial (and temporal) scales. In fact, it is necessary, at the same time, to resolve the IGM inhomogeneities (sub-kpc physical scales), follow the formation of

the very first objects in which PopIII stars form (kpc), the radiative transfer of their ionizing radiation and the transport of their metals (tens of kpc), the build up of various backgrounds (Mpc), and the effects of QSOs (tens of Mpc). Thus, a proper modelling of the relevant physics on these scales, which would enable a direct and simultaneous comparison with all the available data sets mentioned above, would require numerical simulations with a dynamical range of more than 5 orders of magnitude, which is a far cry from the reach of our current computational technology. To overcome the problem, simulations have typically concentrated on trying to explain one (or a few, in the best cases) of the observational constraints. It is therefore difficult from these studies to understand the extent to which their conclusions do not conflict with a different set of experiments other than the one they are considering.

The quest for a more general, data-supported scenario is the main motivation for this study. Although our semi-analytical approach provides a way to achieve this aim in a very straightforward manner and, as we will see, with very satisfactory results, it is important that its uncertainties are kept under control as much as possible. For this reason, we also compare its predictions with those from numerical simulations focusing on a more restricted aspect of the general picture. The final hope is that heavily data-constrained models, like the one presented here, will help us to identify the unique way in which cosmic reionization occurred.

The paper is organized as follows. In the next few sections, we develop the analytical formalism for studying the ionization and thermal history of the IGM, implementing most of the essential physical processes. We discuss the evolution of the ionized regions in Section 2, taking into account the inhomogeneous density distribution of the IGM. The explicit form of the IGM density distribution used in this work is discussed in Section 3. The estimation of the number of ionizing photons from different types of sources is given in Section 4. The formalism for studying the thermal and ionization histories of different phases of the IGM is discussed in Section 5. We discuss some properties of the absorption systems derived from our formalism in Section 6. Finally, we compare the model predictions with various observations and discuss the effect of varying different free parameters in Section 7. The final section presents the summary of our main results, and compares the model with other semi-analytical models and numerical simulations.

2 EVOLUTION OF IONIZED REGIONS

In the following sections, we shall highlight the crucial points of our formalism and try to develop a consistent picture of cosmic reionization, which derives from all known experimental constraints on such a process. Such formalism allows us to track (i) the evolution of the volume filling factors of ionized hydrogen and helium regions, and (ii) the thermal and ionization evolution in each of these regions separately and self-consistently.

2.1 Volume filling factor of ionized regions

Let us first start with individual ionized regions: these can either be singly ionized hydrogen (H II) or doubly ionized helium (He III). We do not consider the analogous He II regions, as typically these match the H II ones and, in any case, very sparse observational data have been collected concerning this ionization state of the IGM. To a first approximation, it is usually assumed that the IGM can be described as an uniform medium with small-scale clumpiness taken into account through a so-called ‘clumping factor’. In such cases,

the evolution of the volume filling factor Q_{HII} for the H II regions will be described by (Shapiro & Giroux 1987)

$$\frac{dQ_{\text{HII}}}{dt} = \frac{\dot{n}_{\text{ph}}}{n_{\text{H}}} - Q_{\text{HII}} C_{\text{HII}} \frac{n_{\text{e}}}{a^3} \alpha_{\text{R}}, \quad (1)$$

where \dot{n}_{ph} is the rate of ionizing photons per unit volume, n_{H} is the hydrogen atoms number density, n_{e} is the electron number density, C_{HII} is the clumping factor for the ionized regions, a is the expansion factor and α_{R} is the recombination coefficient. Under the assumption of homogeneity, the same equation holds for the ionized hydrogen mass fraction as well. One can write a similar equation for the volume filling factor Q_{HeIII} of He III regions too. In this picture, the reionization is said to be complete when individual ionized regions overlap, i.e. $Q_i = 1$. The above equation can be solved given a model for the source term \dot{n}_{ph} and a value for the clumping factor C_i . There are few points worth noting, which are as follows.

(i) The quantity (corresponding to the recombination term on the right-hand side) $Q_{\text{HII}} C_{\text{HII}} n_{\text{e}} n_{\text{H}} \alpha_{\text{R}}$ gives the average recombinations per unit time per unit volume in the universe.

(ii) Also note that we have implicitly assumed that each photon is absorbed shortly after it is emitted, i.e. its mean free path is much smaller than the horizon size (which is true for $z > 2$). In case the photon is able to travel large distances before it is absorbed, one has to take into account the fact that photons might be redshifted below the ionization edge of hydrogen.

(iii) Finally, one should remember that the quantity \dot{n}_{ph} takes into account only those photons that escape into the IGM. The number of photons produced by the source can be much larger; however, a large fraction of those photons will be absorbed in ionizing the high-density halo surrounding the luminous source.

2.2 Inhomogeneous reionization

In the above picture, the inhomogeneities in the IGM are considered simply in terms of the clumping factor in the effective recombination rate without taking into account the density distribution of the IGM. The importance of using a density distribution of the IGM lies in the fact that regions of lower densities will be ionized first and high-density regions will remain neutral for a longer time. The main reason for this is that the recombination rate is higher in high-density regions where dense gas becomes neutral very quickly. Of course, there will be a dependence on how far the high-density region is from an ionizing source. A dense region that is very close to an ionizing source will be ionized quite early compared with, say, a low-density region that is far away from luminous sources.

The first efforts in addressing such issues were carried out by Miralda-Escudé, Haehnelt & Rees (2000; MHR, hereafter). To summarize the main point of this approach, consider, first, the situation where all the individual ionized regions have overlapped (the so-called post-overlap stage; Gnedin 2000). In this scenario, all the low-density regions of the universe will be highly ionized, while there will be some high-density peaks (like the collapsed systems) that will still remain neutral. Thus, as a reasonable first approximation (MHR), we assume that all regions with overdensities $\Delta < \Delta_i$ are ionized (the index i refers to the different ionized species), while regions with $\Delta > \Delta_i$ are completely neutral, with Δ_i increasing as time progresses (i.e. more and more high-density regions are getting ionized). We shall discuss the equation governing the evolution of Δ_i later in this section, while the results for different model parameters will be discussed in Section 7 (see, for example, Fig. 1). Note that, according to this scenario, the reionization is defined to

be completed when all the regions with $\Delta < \Delta_i$ are ionized: one does not need to ionize the whole IGM to complete the reionization process. The effect of this assumption is that only the low-density regions will contribute to the clumping factor (regions whose density is above Δ_i are assumed to be neutral, hence they need not be taken into account while calculating the clumping factor).

The situation is slightly more complicated when the ionized regions are in the pre-overlap stage. At this stage, it is assumed that a volume fraction $1 - Q_i$ of the universe is completely neutral (irrespective of the density), while the remaining Q_i fraction of the volume is occupied by ionized regions. However, within this ionized volume, the high-density regions (with $\Delta > \Delta_i$) will still be neutral. Once Q_i becomes unity, all regions with $\Delta < \Delta_i$ are ionized and the rest are neutral. The high-density neutral regions manifest themselves as the Lyman-limit systems in the QSO absorption spectra. The reionization process after this stage is characterized by an increase in Δ_i : implying that higher density regions are getting ionized gradually.

To develop the equations embedding the above physical picture, we need to know the probability distribution function $P(\Delta) d\Delta$ for the overdensities. We shall discuss the form of $P(\Delta)$ in the next section, but given a $P(\Delta) d\Delta$, it is clear that only a mass fraction

$$F_M(\Delta_i) = \int_0^{\Delta_i} d\Delta \Delta P(\Delta) \quad (2)$$

needs to be ionized, while the remaining high-density regions will be completely neutral because of high recombination rates. The generalization of equation (1), appropriate for this description is given by MHR (see also Wyithe & Loeb 2003)

$$\frac{d[Q_{\text{HII}} F_M(\Delta_{\text{HII}})]}{dt} = \frac{\dot{n}_{\text{ph}}(z)}{n_{\text{H}}} - Q_{\text{HII}} \frac{\alpha_{\text{R}}(T) n_{\text{e}} R(\Delta_{\text{HII}})}{a^3}, \quad (3)$$

where $Q_{\text{HII}} \alpha_{\text{R}}(T) n_{\text{H}} n_{\text{e}} R(\Delta_{\text{HII}})$ gives the number of recombinations per unit time and volume. The factor $R(\Delta_{\text{HII}})$ is analogous to the clumping factor and is given by

$$R(\Delta_{\text{HII}}) = \int_0^{\Delta_{\text{HII}}} d\Delta \Delta^2 P(\Delta). \quad (4)$$

The reionization is complete when $Q_{\text{HII}} = 1$; at this point, a mass fraction $F_M(\Delta_{\text{HII}})$ is ionized, while the rest is (almost) completely neutral.

Note that there are two unknowns Q_{HII} and $F_M(\Delta_{\text{HII}})$ in equation (3) (and similarly for the He III regions). For the post-overlap stage, we put $Q_i = 1$ and can solve the equation for Δ_i . However, for the pre-overlap stage, we have to deal with both the unknowns and it is thus impossible to solve it without more assumptions. One can fix either Δ_i or F_M (the ionized mass fraction). There is no obvious way of dealing with this problem. In this work, we assume that Δ_i does not evolve with time in the pre-overlap stage, i.e. it is equal to a critical value Δ_c . To fix this Δ_c , we note that results do not vary considerably as Δ_c is varied from ~ 10 to ~ 100 . For definiteness, we take the value corresponding to the typical overdensity of collapsed haloes at the virial radius. The exact value of this overdensity depends on the density profile of the halo; it can be shown that it is ≈ 59.2 for an isothermal profile, while it is ≈ 63.7 for the Navarro, Frenk & White (NFW; Navarro, Frenk & White 1996) profile. In this paper, we can safely assume $\Delta_c = 60$, and also assume that this critical value is the same for H II and He III. Once Δ_i is fixed, one can follow the evolution of Q_i until it becomes unity. Following that, we enter the post-overlap stage, where the situation is well-described by equation (1).

3 PROBABILITY DISTRIBUTION $P(\Delta)$

There can be various approaches to determine the density distribution of the IGM at various redshifts. It is clear that various complicated physical processes will not allow us to obtain a simple distribution from analytical calculations. One has to resort to either simulations, or some sort of approximation schemes. In the approach followed by MHR, one uses a density distribution inspired by hydrodynamical simulations. While such approaches are widely used, one should keep in mind that the limitations related to box size and resolution are inherent to every simulation. On the other hand, there are approaches where the density distribution is obtained from some approximation schemes. These approximation schemes seem to be reasonable in the linear or quasi-linear regime of density fluctuations, while they are more inaccurate when non-linear effects creep in.

In this work, we shall use such an approximation to describe the low-density IGM. There are several reasons to believe that the low-density regions of the IGM are well described by the lognormal distribution (see, for example, Choudhury, Padmanabhan & Srianand 2001b; Choudhury, Srianand & Padmanabhan 2001a; Viel et al. 2002), which is shown to be in excellent agreement with numerical simulations (Bi & Davidsen 1997). However, the lognormal distribution seems to fail at very high densities (say, when the densities are typical to that of collapsed haloes). To see this, note that at high densities ($\Delta \gg 1$), the lognormal distribution has the limiting form $P(\Delta) \sim \Delta^{-\ln \Delta / \sigma^2 - 1}$, whereas it is expected that it should follow a simple power-law $P(\Delta) \sim \Delta^\beta$. In fact, if dark matter haloes have a density profile of the form $r^{3/(\beta+1)}$, then it can be shown that $P(\Delta)$ should fall as Δ^β . For an isothermal profile, one has $\beta = -2.5$, while for an NFW profile, the value of β varies from -4 in the centre of the halo to -2 at the virial radius.

We thus assume the probability distribution of the overdensities to be lognormal at low densities, changing to a power-law form at high densities:

$$P(\Delta) = \frac{A}{\sigma \Delta \sqrt{2\pi}} e^{-\frac{1}{2\sigma^2} (\ln \Delta - \mu)^2}$$

if $\Delta < \Delta_V$,

$$P(\Delta) = \frac{A}{\sigma \Delta_V \sqrt{2\pi}} e^{-\frac{1}{2\sigma^2} (\ln \Delta_V - \mu)^2} \left(\frac{\Delta}{\Delta_V} \right)^\beta$$

if $\Delta > \Delta_V$,

(5)

where σ is the rms linear mass fluctuations in baryons.¹ If we want the derivative of $P(\Delta)$ to be continuous at the transition overdensity Δ_V , then it follows that the slope β and Δ_V must be related by

$$-1 - \frac{1}{\sigma^2} (\ln \Delta_V - \mu) = \beta. \quad (6)$$

The parameters A and μ are determined by normalizing the volume and mass to unity. In most cases, the power-law form of the probability distribution comes into effect only for the post-overlap phase.

In general, haloes could have β varying with the distance from the centre depending on the density profile. Simulations also suggest a redshift evolution of β , with $\beta = -2.5$ at high redshifts, while it is

¹ Throughout this paper, we will assume a flat universe with total matter, vacuum and baryonic densities in units of the critical density of $\Omega_m = 0.27$, $\Omega_\Lambda = 0.73$ and $\Omega_b h^2 = 0.024$, respectively, and a Hubble constant of $H_0 = 100 h \text{ km s}^{-1} \text{ Mpc}^{-1}$, with $h = 0.72$. The parameters defining the linear dark matter power spectrum are $\sigma_8 = 0.9$, $n = 0.99$, $dn/d \ln k = 0$.

≈ -2.2 at redshifts around 2 (Miralda-Escudé et al. 1996). In this work, however, we assume a constant value of -2.3 independent of the redshift and the distance from the centre. This is reasonable as long as we are not too close to the centre of the halo; also most of the results are insensitive to β as long it is within the range $[-2.2, -2.5]$. Given a value of β , the value of Δ_V will, in general, evolve with time.

To proceed further in the solution of equation (3), one has to estimate two quantities: (i) the photon production rate, $\dot{n}_{\text{ph}}(z)$, and (ii) the temperature, T , of the ionized regions. We discuss the method adopted to obtain these estimates in the next sections.

4 PHOTON PRODUCTION RATE

4.1 Photons from galaxies

One can use the Press–Schechter formalism to estimate the mass function of dark matter haloes of mass M that collapsed at a redshift z_c . In this paper, we shall use the formalism of Sasaki (1994) for calculating the formation and merging rates of dark matter haloes. Assuming a model where the star formation rate (SFR) peaks around the dynamical time-scale of the halo, it will form stars at the rate (Chiu & Ostriker 2000; Choudhury & Srianand 2002)

$$\dot{M}_{\text{SF}}(M, z, z_c) = \epsilon_{\text{SF}} \left(\frac{\Omega_b}{\Omega_m} M \right) \frac{t(z) - t(z_c)}{t_{\text{dyn}}^2(z_c)} e^{-\frac{t(z) - t(z_c)}{t_{\text{dyn}}(z_c)}}, \quad (7)$$

where ϵ_{SF} is the efficiency of star formation. We can then write the cosmic SFR per unit comoving volume at a redshift z ,

$$\dot{\rho}_{\text{SF}}(z) = \int_z^\infty dz_c \int_{M_{\text{min}}(z_c)}^\infty dM \dot{M}_{\text{SF}}(M, z, z_c) N(M, z, z_c), \quad (8)$$

where $N(M, z, z_c) dM dz_c$ gives the number of haloes within a mass range $(M, M + dM)$ formed within a redshift interval $(z_c, z_c + dz_c)$ and surviving down to redshift z . The lower integration limit, $M_{\text{min}}(z_c)$, takes into account the fact that low-mass haloes will not be able to cool and form stars. Also, note that we do not take into account possible disruption of star-forming haloes due to energy injection from exploding supernovae. We shall discuss the choice of $M_{\text{min}}(z_c)$ in detail in a later section.

Putting all the relevant expressions together, one can write the cosmic SFR in a neater form:

$$\dot{\rho}_{\text{SF}}(z) = \bar{\rho}_b \frac{1}{D(z)} \int_z^\infty dz_c \epsilon_{\text{SF}} F_1(z, z_c) \mathcal{I}(z_c), \quad (9)$$

where $\bar{\rho}_b$ is the mean baryonic density, and where

$$F_1(z, z_c) = \left[\frac{\dot{D}(z_c)}{D(z_c)H(z_c)} \right] \frac{D(z_c)}{(1+z_c)} \frac{t(z) - t(z_c)}{t_{\text{dyn}}^2(z_c)} e^{-\frac{t(z) - t(z_c)}{t_{\text{dyn}}(z_c)}} \quad (10)$$

and

$$\mathcal{I}(z_c) = \int_{v(M_{\text{min}}(z_c))}^\infty dv \left(\sqrt{\frac{2}{\pi}} e^{-v^2/2} \right) v^2. \quad (11)$$

In the above expressions, $D(z)$ gives the linear growth factor of dark matter perturbations and $v(M) = \delta_c / [D(z)\sigma_{\text{DM}}(M)]$. In this paper, we fix the critical overdensity for collapse, δ_c , to 1.69.

The rate of ionizing photons per unit volume per unit frequency range would be

$$\dot{n}_{\nu, G}(z) = \left[\frac{dN_\nu}{dM} \right] \bar{\rho}_b \frac{1}{D(z)} \int_z^\infty dz_c \epsilon_{\text{SF}} f_{\text{esc}} F_1(z, z_c) \mathcal{I}(z_c), \quad (12)$$

where f_{esc} is the escape fraction of ionizing photons from the star-forming haloes and dN_ν/dM gives the number of photons emitted

per frequency range per unit mass of stars. Given the spectra of stars of different masses in a galaxy and their initial mass function (IMF), this quantity can be computed in a straightforward way. The IMF and spectra will depend on the details of star formation and metallicity, and can be quite different for Pop II and Pop III stars. We shall return to this point at the end of this section. Given the above quantity, it is straightforward to calculate the total number density of ionizing photons emitted at a particular frequency range $[\nu_{\min}, \nu_{\max}]$ by galaxies per unit time.

4.2 Ionizing photons from PopII/PopIII stars

While considering the number of photons from stars, one has to keep in mind that the nature of stars that were formed early could be very different from what we observe at lower redshifts. The physical motivation behind this assumption is the commonly accepted view that early stars are metal-free and hence the IMF would be top-heavy, i.e. dominated by high-mass stars (Schneider et al. 2002). Currently, the observational support for this assumption comes mainly from the analysis of the cosmic NIRB data (Magliocchetti et al. 2003; Salvaterra & Ferrara 2003). Hence, in this work we consider the possibility that, at early redshifts, a population of metal-free, massive (PopIII) stars produced a large number of photons. On the other hand, star formation at low redshifts, as we know, is dominated by high metallicity PopII stars with the usual Salpeter-like IMF. It is believed that the transition from PopIII to PopII stars occurred because of an increase in the metallicity in the active star-forming regions above a critical value of $Z_{\text{crit}} = 10^{-5 \pm 1} Z_{\odot}$. However, it is not clear how abrupt the transition has been, due to the poorly known amplitude of the optical background at 0.6–0.8 μm . We shall therefore denote this transition redshift by z_{trans} and study the effects of its variation. We should mention that PopIII star formation may continue at lower redshifts with a decreasing rate, however the interpretation of the NIRB requires that their contribution to the ionizing flux be negligible with respect to the PopII stars. Although some metal pollution has to take place for transition to PopII stars, it is necessary that the majority of the NIRB-contributing PopIII stars have masses such that a black hole is the final product of their evolution (Salvaterra & Ferrara 2003).

From the above, it thus turns out that the star formation is made up of two components:

$$\dot{n}_{\text{ph},G}(z) = \dot{n}_{\text{ph,PopII}}(z) + \dot{n}_{\text{ph,PopIII}}(z); \quad (13)$$

the previous expression involves two free parameters, which are the ionizing photon efficiencies of the PopII and PopIII stars, namely, $\epsilon_{\text{PopII}} \equiv \epsilon_{\text{SF,PopII}} f_{\text{esc,PopII}}$ and $\epsilon_{\text{PopIII}} \equiv \epsilon_{\text{SF,PopIII}} f_{\text{esc,PopIII}}$. We assume that the stellar population within the galaxies formed at $z > z_{\text{trans}}$ is dominated by PopIII stars, while at lower redshifts it is dominated by PopII stars. Because the SFR peaks at the dynamical time-scale after the formation of the halo and decreases exponentially thereafter, the formation rate of PopIII stars continues for some amount of time after z_{trans} and hence the transition is not instantaneous. By this assumption, we are implicitly neglecting the effects of galactic self-enrichment on the IMF transition. Although locally (i.e. inside a given galaxy), the transition from PopIII to PopII star formation mode can occur at epochs different (either earlier or later) than z_{trans} , the studies of NIRB data set the epoch when the bulk of the cosmic stars became PopII at z_{trans} .

To calculate the number of photons produced per unit mass of PopII star formed $[dN_{\nu}/dM]_{\text{PopII}}$, we use the stellar spectra calcu-

lated using STARBURST99² (Leitherer et al. 1999), with metallicity $Z = 0.001 = 0.05 Z_{\odot}$ and standard Salpeter IMF. The number of photons per unit mass of star formed, when integrated over appropriate frequencies, gives $(8.05, 2.62, 0.01) \times 10^{60} M_{\odot}^{-1}$ for (H II, He II, He III) respectively. For calculating $[dN_{\nu}/dM]_{\text{PopIII}}$, we first assume that the IMF of the PopIII stars is dominated by very high mass stars. Because the number of photons produced per unit mass of stars formed is somewhat independent of the stellar mass for high-mass stars, it is independent of the precise shape of the IMF (as long as the IMF is dominated by high-mass stars). The value of $[dN_{\nu}/dM]_{\text{PopIII}}$ is calculated using stellar spectra for high-mass stars ($\geq 300 M_{\odot}$) as given by Schaerer (2002). When integrated over appropriate frequencies, this quantity is equal to $(2.69, 4.46, 1.36) \times 10^{61} M_{\odot}^{-1}$ for (H II, He II, He III) respectively.

4.3 The minimum mass for the star-forming haloes

The quantity $M_{\min}(z_c)$ in equation (8) depends on the cooling efficiency of haloes. We assume that molecular cooling is active at high redshifts and $M_{\min}(z_c)$ increases with decreasing z (Fuller & Couchman 2000). However, it is also possible that the molecular cooling within the minihaloes could be highly suppressed due to photodissociation of hydrogen molecules. We shall study the effect of minihalo suppression in Section 7.5. At lower redshifts (say $z < 10$), when the mass function of collapsed haloes is dominated by relatively high-mass haloes, the SFR is more or less independent of whether molecular cooling is effective or not.

There is a further factor that needs to be taken into account: the radiative feedback from stars. Once the first galaxies form stars, their radiation will ionize and heat the surrounding medium, increasing the mass scale (often referred to as the filtering mass) above which baryons can collapse into haloes within those regions. The minimum mass of haloes that are able to cool is thus much higher in ionized regions than in neutral ones. Because we are considering a multiphase IGM, one needs to take into account the heating of the ionized regions from the beginning (even before the actual overlap has started). As we compute the temperature of the ionized region self-consistently, we can calculate the minimum circular velocity of haloes that are able to cool using the relation

$$v_c^2 = \frac{2k_{\text{boltz}}T}{\mu m_p}, \quad (14)$$

where μ is the mean molecular weight: $\mu m_p = \rho_b/n_b$; m_p is the proton mass, and n_b is the number density of baryons. Typically, for a temperature of 3×10^4 K, the minimum circular velocity is ~ 30 – 50 km s⁻¹, which is comparable to the filtering scale obtained from numerical simulations of Gnedin (2000) after the universe has reionized.

Note that the above value of v_c will evolve according to the temperature of the gas. An alternative feedback prescription is to fix the minimum circular velocity of haloes allowed to form stars at a given value, which can be taken to be in the range $v_c = 35$ – 50 km s⁻¹ (Gnedin 2000; Kitayama et al. 2001). We shall explore the effect of such different feedback prescriptions later in Section 7.

4.4 Photons from QSOs

In order to calculate the number of ionizing photons from QSOs, we shall follow the simple formalisms developed by Wyithe & Loeb (2003) and Mahmood, Devriendt & Silk (2005). The only difference

² <http://www.stsci.edu/science/starburst99>

in our approach is that we use a different prescription for calculating the merging and formation of dark matter haloes. In the previous works, the merging rates of dark matter haloes were based on the formalism by Lacey & Cole (1993), while our model uses the Sasaki (1994) methodology. For the reason of completeness, we include the details of the model for calculating the luminosity function of QSOs in this section.

The key assumption to calculate the luminosity of QSOs is that the mass of the accreting black hole M_{bh} is correlated with the circular velocity v_c of the collapsed halo through the relation

$$M_{\text{bh}} = \epsilon v_c^\alpha. \quad (15)$$

It is argued that $\alpha = 5$ in a self-regulated growth of supermassive black holes (Silk & Rees 1998), a value found to match observations of the local universe.

It is then reasonable to assume that the black hole radiates with the Eddington luminosity (in the B band), given by

$$\frac{L_B}{L_{\odot,B}} = 5.7 \times 10^3 \frac{M_{\text{bh}}}{M_{\odot}}, \quad (16)$$

which gives

$$\frac{L_B}{L_{\odot,B}} = \beta \left(\frac{M}{M_{\odot}} \right)^{\alpha/3}, \quad (17)$$

where we have used the relation between the circular velocity and the mass of a virialized halo (Choudhury & Padmanabhan 2002) to obtain

$$\beta = 5.7 \times 10^3 \epsilon_0 10^{-4\alpha} \left[\frac{H_0^2 18\pi^2}{H^2(z) \Delta_{\text{vir}}(z)} \right]^{\alpha/6} \times \left[1 - \frac{2\Omega_\Lambda H_0^2}{3H^2(z) \Delta_{\text{vir}}(z)} \right]^\alpha h^{\alpha/3} \quad (18)$$

with

$$\epsilon_0 = \frac{\epsilon (159.4 \text{ km s}^{-1})^\alpha}{M_{\odot}}. \quad (19)$$

Note that, even if the black hole radiates at a sub-Eddington rate, the corresponding uncertainty can be absorbed into the value of β . The luminosity function of QSOs (i.e. the number of QSOs per unit comoving volume per unit luminosity range) will be given by

$$\psi(L_B, z) dL_B = \int_{\infty}^z dz_c N(M, z, z_c) dM, \quad (20)$$

where M and L_B are related by equation (17). If we assume that each QSO lives for a time $t_{\text{qso}}(z) \ll (\dot{a}/a)^{-1}$, then the QSO activity can be taken to be almost instantaneous and we can approximate

$$\int_{\infty}^z dz_c N(M, z, z_c) \approx \frac{dz}{dt} t_{\text{qso}}(z) N(M, z, z). \quad (21)$$

Then

$$\begin{aligned} \psi(L_B, z) &= \frac{dz}{dt} t_{\text{qso}}(z) N(M, z, z) \frac{dM}{dL_B} \\ &= \frac{3}{\alpha L_B} M N_M(z) v^2 \left[\frac{\dot{D}(z)}{D(z) H(z)} \right] H(z) t_{\text{qso}}(z). \end{aligned} \quad (22)$$

We fix $t_{\text{qso}}(z) = 0.035 t_{\text{dyn}}(z)$ (Mahmood et al. 2005). Given $\alpha = 5$, one can fix the free parameter ϵ_0 by comparing the model with observations of QSO luminosity function.

This simple procedure works very well at intermediate and high redshifts, but fails to match the observations at low redshifts. One can introduce a phenomenological function in equation (22) to take into

account the break in the luminosity function at high luminosities. We find that a modified $\psi(L_B, z)$ of the form (Mahmood et al. 2005)

$$\psi(L_B, z) \rightarrow \psi(L_B, z) \exp \left(- \frac{M}{10^{11.25+z} M_{\odot}} \right) \quad (23)$$

is good enough in matching the low-redshift observations. This cut-off is at very high luminosities and has virtually no effect at $z > 3$.

Given the luminosity function, the rate of ionizing photons from QSOs per unit volume per unit frequency range will be

$$\dot{n}_{\nu, Q}(z) = \int_0^{\infty} dL_B \psi(L_B, z) \frac{L_\nu(L_B)}{h_p \nu}, \quad (24)$$

where h_p is Planck's constant. We next use the mean UV QSO spectrum (Schirber & Bullock 2003)

$$\frac{L_\nu(L_B)}{\text{erg s}^{-1} \text{ Hz}^{-1}} = \frac{L_B}{L_{\odot,B}} 10^{18.05} \left(\frac{\nu}{\nu_H} \right)^{-1.57}, \quad (25)$$

which then gives

$$\begin{aligned} \dot{n}_{\nu, Q}(z) &= \left[\frac{10^{18.05} \text{ erg s}^{-1} \text{ Hz}^{-1}}{L_{\odot,B}} \right] \frac{1}{h_p \nu_H} \left(\frac{\nu}{\nu_H} \right)^{-2.57} \\ &\times \int_0^{\infty} dL_B L_B \psi(L_B, z). \end{aligned} \quad (26)$$

The rate of ionizing photons from QSOs is obtained simply by integrating over all relevant frequencies.

This simple phenomenological model suits very nicely the purposes of this paper. Alternatively, one can simply use the observed luminosity function for QSOs for calculating the number of ionizing photons. Because the above model matches perfectly well with observations at low redshifts, none of the results would be affected. At high redshifts, say $z > 6$, the contribution from QSOs is negligible compared with that of galaxies and can be ignored.

5 THERMAL EVOLUTION

In the previous sections, we have discussed the evolution of the ionized volume filling factors and various physical quantities related to them. It is clear that the baryonic universe will behave as a three-phase medium constituted by: (i) completely neutral regions, (ii) regions where hydrogen is ionized and helium is singly ionized, and (iii) a region where both species are fully ionized. We have assumed that the ionization front for the doubly ionized helium can never overtake that for ionized hydrogen, which is found to be always true for the type of spectra we are using for the ionizing sources (note that a much harder spectrum can always make the ionization front for the doubly ionized helium leading the ionized hydrogen region).

The thermal evolution equations are solved separately for each of the three regions. In the absence of heating sources, the evolution is nearly trivial for the neutral region, with the temperature decreasing adiabatically. However, there is always a background of hard photons that can heat the neutral IGM. Because the temperature of the neutral region hardly affects the reionization history, we ignore such hard photons and let the temperature of the neutral regions decrease adiabatically. In the ionized regions, the temperature can be calculated using the dynamical equation

$$\begin{aligned} \frac{dT}{dt} &= -2H(z)T - \frac{T}{\sum_i X_i} \frac{d\sum_i X_i}{dt} \\ &+ \frac{2}{3k_{\text{boltz}} n_b (1+z)^3} \frac{dE}{dt}, \end{aligned} \quad (27)$$

where

$$X_i \equiv \frac{n_i m_p}{\bar{\rho}_b} \quad (28)$$

and dE/dt gives the net heating rate per baryon. For most purposes, it is sufficient to take into account the photoionization heating and recombination cooling [and Compton cooling of cosmic microwave background (CMB) photons, which can be important at high redshifts]. For example, in the regions where only hydrogen is ionized, we have

$$\frac{dE}{dt} = n_{\text{HI}}(1+z)^6 \int_{\nu_{\text{H}}}^{\infty} d\nu \lambda_{\text{H}}(z; \nu) \frac{\dot{n}_\nu(z)}{Q_{\text{HI}}(z)} \sigma_{\text{H}}(\nu) h_p(\nu - \nu_{\text{H}}) - R(\Delta_{\text{HI}}) \alpha_{\text{RC}}(T) n_{\text{HI}} n_e (1+z)^6 \quad (29)$$

where α_{RC} is the recombination cooling rate, $\lambda_{\text{H}}(z; \nu)$ is the proper mean free path for hydrogen ionizing photons with frequency $\nu > \nu_{\text{H}}$. It is found from observations at low redshifts that $\lambda_{\text{H}}(z; \nu) \propto \nu^{1.5}$; this is understood from the frequency-dependence of the absorption cross-section $\sigma_{\text{H}}(\nu) \propto \nu^{-3}$ and the column density distribution of QSO absorption lines $dN/dN_{\text{HI}} \propto N_{\text{HI}}^{-3/2}$ (Petitjean et al. 1993). We assume this relation to be valid for all redshifts. Note that this frequency dependence of the mean free path hardens the ionizing spectrum. However, at frequencies below the ionization threshold of He II, the diffuse recombination radiation from the IGM tends to compensate for this hardening (Haardt & Madau 1996). Given this, we assume $\lambda_{\text{H}}(z; \nu) = \lambda_{\text{H},0}(z)$ for $\nu \leq \nu_{\text{HeII}}$ and $\lambda_{\text{H}}(z; \nu) = \lambda_{\text{H},0}(z) (\nu/\nu_{\text{HeII}})^{1.5}$ for $\nu > \nu_{\text{HeII}}$. The procedure for calculating $\lambda_{\text{H},0}(z) \equiv \lambda_{\text{H}}(z; \nu = \nu_{\text{H}})$ is described in the next section.

The equation for evolution of the temperature has to be supplemented by those for the ionization of the individual species. In the most general case, one has three independent species $X_i = \{X_{\text{HI}}, X_{\text{HeI}}, X_{\text{HeIII}}\}$, with other species being given by

$$\begin{aligned} X_{\text{HI}} &= 1 - Y - X_{\text{HeI}}, \\ X_{\text{HeII}} &= \frac{Y}{4} - X_{\text{HeI}} - X_{\text{HeIII}}, \\ X_e &= X_{\text{HI}} + X_{\text{HeII}} + 2X_{\text{HeIII}}, \end{aligned} \quad (30)$$

where $Y = 0.24$ is the helium weight fraction. For example, the evolution of X_{HI} in the H II region is given by

$$\frac{dX_{\text{HI}}}{dt} = -X_{\text{HI}}(1+z)^3 \int_{\nu_{\text{H}}}^{\infty} d\nu \lambda_{\text{H}}(z; \nu) \frac{\dot{n}_\nu(z)}{Q_{\text{HI}}(z)} \sigma_{\text{H}}(\nu) + R(\Delta_{\text{HI}}) \alpha_{\text{R}}(T) X_{\text{HI}} X_e \frac{\bar{\rho}_b}{m_p} (1+z)^3. \quad (31)$$

Similar equations, though slightly more complicated, can be written down for other regions too.

In passing, note that the volume emissivity is given by

$$\epsilon_\nu(z) = \dot{n}_\nu(z) h_p \nu (1+z)^3, \quad (32)$$

while the ionizing flux for a particular species i (one of H I, He I or He II) is given by

$$J_\nu(z) \equiv \frac{\lambda_i(z; \nu)}{4\pi} \epsilon_\nu(z) = \frac{\lambda_i(z; \nu)}{4\pi} \dot{n}_\nu(z) h_p \nu (1+z)^3. \quad (33)$$

The photoheating rate for a particular species is given by

$$\begin{aligned} \Gamma_{\text{PH}}(z) &= 4\pi \int_{\nu_{\text{min}}}^{\infty} d\nu \frac{J_\nu}{h_p \nu} \sigma_i(\nu) h_p (\nu - \nu_{\text{min}}) \\ &= (1+z)^3 \int_{\nu_{\text{min}}}^{\infty} d\nu \lambda_i(z; \nu) \dot{n}_\nu(z) \sigma_i(\nu) h_p (\nu - \nu_{\text{min}}), \end{aligned} \quad (34)$$

where ν_{min} is the threshold frequency for the species considered. The photoionization rate is given by

$$\begin{aligned} \Gamma_{\text{PI}}(z) &= 4\pi \int_{\nu_{\text{min}}}^{\infty} d\nu \frac{J_\nu}{h_p \nu} \sigma_i(\nu) \\ &= (1+z)^3 \int_{\nu_{\text{min}}}^{\infty} d\nu \lambda_i(z; \nu) \dot{n}_\nu(z) \sigma_i(\nu). \end{aligned} \quad (35)$$

Note that we have included the clumping term $R(\Delta_i)$ in the expressions (29) and (31). As more and more regions of higher densities get ionized, the value of $R(\Delta_i)$ becomes larger which, in turn, gives a larger value of the temperature. Thus the temperature T of the ionized regions obtained from the above system of equations are essentially weighted by the mass of the corresponding regions. In this sense, one can assume T to be an estimate of the mass-averaged temperature of the region. We should emphasize that T is not the rigorously defined mass-averaged temperature, but should be considered as a simple approximation in the ionized regions. If the quantities T and X_i defined in this section are approximate estimates of the mass-averaged values in the ionized region, then the global mean values T_{global} and $X_{\text{global},i}$ can be obtained by weighted averages over different regions, according to the mass fraction of the corresponding region. Also, note that the above T is not same as the conventional T_0 , which is defined as the temperature of gas at the mean IGM density ($\Delta = 1$). Similarly, the ionization fractions defined above need not correspond to the values at the mean density. The values at the mean density (i.e. T_0 , $X_{\text{HI},0}$) can be solved using the same equations (27) and (31), but without putting in the clumping factor $R(\Delta_{\text{HI}})$, i.e.

$$\begin{aligned} \frac{dT_0}{dt} &= -2H(z)T_0 - \frac{T_0}{\sum_i X_{i,0}} \frac{d\sum_i X_{i,0}}{dt} \\ &\quad + \frac{2}{3k_{\text{boltz}} n_b} \left[n_{\text{HI},0} \frac{\Gamma_{\text{PH}}(z)}{Q_{\text{HI}}(z)} - \alpha_{\text{RC}}(T_0) n_{\text{HI},0} n_{e,0} (1+z)^3 \right] \end{aligned} \quad (36)$$

and

$$\frac{dX_{\text{HI},0}}{dt} = -X_{\text{HI},0} \frac{\Gamma_{\text{PI}}(z)}{Q_{\text{HI}}(z)} + \alpha_{\text{R}}(T_0) X_{\text{HI},0} X_{e,0} \frac{\bar{\rho}_b}{m_p} (1+z)^3. \quad (37)$$

5.1 Mean free path for photons

The mean free path for ionizing photons depends on the size and topology of the ionized regions. Hence, for a self-consistent calculation of the mean free path, one has to use the evolution of the volume filling factor of the ionized regions. Note that we only have statistical information about the fraction of volume and mass that is ionized, i.e. we do not calculate the size of individual ionized regions.

Given this situation, we use a simple model developed by MHR to calculate the mean free path $\lambda_{i,0}(z)$ for photons (at $\nu = \nu_{\text{H}}$). As discussed in MHR, their method is a good approximation when a very high fraction of volume is ionized. It is clear that a photon will be able to travel through the low-density ionized volume

$$F_V(\Delta_i) = \int_0^{\Delta_i} d\Delta P(\Delta) \quad (38)$$

before being absorbed. In the simple model, one assumes that the fraction of volume filled up by the high-density regions is $1 - F_V$, hence their size is proportional to $(1 - F_V)^{1/3}$, and the separation between them along a random line of sight will be proportional to $(1 - F_V)^{-2/3}$, which, in turn, will determine the mean free path. Then one has

$$\lambda_{i,0}(z) = \frac{\lambda_0}{[1 - F_V(\Delta_i)]^{2/3}}, \quad (39)$$

where we can fix λ_0 by comparing with low-redshift observations. In fact, it has been suggested (from simulations and structure formation arguments; MHR) that λ_0 should be determined by the Jeans length which, in turn, is determined by the minimum circular velocity for star-forming haloes (equation 14):

$$x_b(z) = H_0^{-1} v_c \sqrt{\frac{\gamma}{3\Omega_m(1+z)}}, \quad (40)$$

where γ is the adiabatic index. In this work, we assume $\lambda_0 \propto x_b(z)$, with the proportionality constant being determined by comparing with low-redshift observations. The mean free path for photons at $\nu = \nu_H$ is given by the typical separation between the Lyman-limit systems, which is observed to be ~ 33 Mpc at $z = 3$. From the knowledge of $\lambda_{i,0}(z)$, one can then predict the number of Lyman-limit systems per unit redshift range through the relation (Madau, Haardt & Rees 1999; Miralda-Escudé 2003)

$$\frac{dN_{LL}}{dz} = \frac{c}{\sqrt{\pi} \lambda_{i,0}(z) H(z) (1+z)}, \quad (41)$$

which can be directly compared with available observations at $2 < z < 4$.

6 PROPERTIES OF ABSORPTION SYSTEMS

In this section, we discuss how to obtain some of the properties of the IGM when they are observed in the absorption spectra of QSOs.

Given the probability distribution, the estimates of the temperature, T , and of the neutral hydrogen density n_{HI} , we can compute the mean transmitted flux as will be observed in the absorption spectra of QSOs. The optical depth at a given point is given by

$$\tau(\mathbf{x}, z) = I_\alpha n_{HI}(\mathbf{x}, z) (1+z)^3 \frac{c}{H(z)}, \quad (42)$$

where $I_\alpha = 4.45 \times 10^{-18} \text{ cm}^{-2}$ is a constant. It is natural to assume that the matter and radiation in the IGM are in photoionization equilibrium; in that case, the neutral hydrogen density is related to the baryonic overdensity through

$$n_{HI}(\mathbf{x}, z) = n_{HI,0}(z) \Delta^{2.7-0.7\gamma}(\mathbf{x}, z). \quad (43)$$

The optical depth in the ionized region will then be

$$\tau(\mathbf{x}, z) = A(z) \Delta^{2.7-0.7\gamma}(\mathbf{x}, z), \quad (44)$$

where

$$A(z) = I_\alpha n_{HI,0}(z) (1+z)^3 \frac{c}{H(z)}. \quad (45)$$

In general, one should use the global average value of $n_{HI,0}(z)$ in the above expression, taking into account the neutral and different ionized regions. The transmitted flux is

$$F(\mathbf{x}, z) \equiv e^{-\tau(\mathbf{x}, z)}, \quad (46)$$

with its global mean given by

$$F(z) = \int_0^{\Delta_{HII}} d\Delta e^{-A(z)\Delta^{2.7-0.7\gamma}} P(\Delta). \quad (47)$$

The equation of state (EOS) can be written in terms of the adiabatic index as $T \propto \Delta^{\gamma-1}$; note that, sometimes and somewhat confusing, γ rather than $\gamma - 1$ is defined as the slope of the temperature-density relation. It is, in principle, possible to compute the value of γ by studying the evolution of the temperature for fluid elements of different densities. However, such a study is somewhat beyond the

scope of this paper and will be reported somewhere else. As far as this work is concerned, we keep γ as a free parameter varying in the range $1 \leq \gamma \leq 2.4$ and compute the transmitted flux over a wide range of values of γ . Note that the choice of γ does not affect any of our other results.

Another quantity that can be readily estimated from our models is the optical depth of CMB photons due to Thomson scattering with free electrons. This can be written as

$$\tau_{el}(z) = \sigma_T c \int_0^{z(t)} dt n_{\text{global,e}} (1+z)^3, \quad (48)$$

where $n_{\text{global,e}}$ is the global average value of the comoving electron density. We neglect additional small contributions to τ_{el} arising from early X-ray sources, but we do include relic free electrons from cosmic recombination (Venkatesan, Giroux & Shull 2001).

7 RESULTS

In this section, we present the main results for our model along with their interpretation. In the first part, we analyse what we consider the ‘fiducial’ model in terms of the choice of free parameters and confront it with observations. We shall see that this ‘fiducial’ model seems to match all the available experimental data, thus justifying our analysis.

The two main free parameters of the model are the ionizing efficiencies of the two stellar populations, both of which are quite uncertain. For ‘normal’ PopII stars, the fiducial values are taken to be $\epsilon_{\text{SF,PopII}} = 0.1$, which is partly constrained by low-redshift observations of the cosmic SFR (Nagamine et al. 2004), and $f_{\text{esc}} = 0.5$ per cent, yielding $\epsilon_{\text{PopII}} = 0.05$ per cent. The estimates of the escape fraction are quite uncertain and we shall discuss the effects of its variation later on.

For the metal-free PopIII stars, the best observational constraints come from the excess in the cosmic NIRB data (Magliocchetti et al. 2003; Salvaterra & Ferrara 2003), which imply an upper limit on the combination $\epsilon_{\text{SF,PopIII}} (1 - f_{\text{esc}}) \equiv \epsilon_{\text{SF,PopIII}} - \epsilon_{\text{PopIII}} \leq 0.1$ for a top-heavy IMF. However, this is not sufficient to constrain ϵ_{PopIII} . It is found that for low-mass haloes ($M \sim 10^6 M_\odot$), the escape fraction can be as high as $f_{\text{esc}} \approx 0.95$ (Whalen, Abel & Norman 2004), while it can be significantly low for high-mass haloes (Ricotti & Shull 2000; Kitayama et al. 2004). Because the mass function of collapsed haloes is dominated by low-mass haloes at high redshifts, it is reasonable to use high values of f_{esc} , particularly before reionization. Once the IGM is ionized, the star formation in low-mass haloes is suppressed and hence one should probably use a lower value for the escape fraction appropriate for haloes of higher mass. Similarly there are no strong (theoretical or observational) constraints on the value of $\epsilon_{\text{SF,PopIII}}$. Hence, for simplicity, we ignore any redshift or mass-dependence of f_{esc} and $\epsilon_{\text{SF,PopIII}}$, and use the fiducial values $\epsilon_{\text{SF,PopIII}} = 0.8$ per cent and $f_{\text{esc}} = 90$ per cent so that $\epsilon_{\text{PopIII}} = 0.7$ per cent. Note that all our results (except the SFR) are sensitive only to the combination $\epsilon_{\text{SF,PopIII}} f_{\text{esc}}$. Hence one can vary the individual values of the two parameters keeping the value of ϵ_{PopIII} the same and still obtain identical results for the reionization history. For example, low-mass haloes might have $f_{\text{esc}} \approx 1$; this implies that our fiducial model requires a star-forming efficiency of $\epsilon_{\text{SF,PopIII}} = 0.7$ per cent. On the other hand, in the ionized regions (where the mass function is dominated by higher mass haloes), the escape fraction could be significantly lower (say, $f_{\text{esc}} \approx 10$ per cent); consequently, the implied value of the star-forming efficiency in our fiducial model would be $\epsilon_{\text{SF,PopIII}} = 7$ per cent, which is probably higher than the theoretical expectations, but still does not violate

the upper limit from NIRB data. However, if the escape fraction is significantly lower than this, it can be quite difficult to match the NIRB data and reionization constraints simultaneously. The effects of varying ϵ_{PopIII} will be discussed later.

Finally, the value of the transition redshift z_{trans} is taken to be 10, which seems to be favoured by NIRB observations. The best-fitting value $z_{\text{trans}} = 8.8$ (Salvaterra & Ferrara 2003) obtained for a burst-like mode of SFR might be somewhat larger when we allow the PopIII SFR to decrease exponentially even after $z = z_{\text{trans}}$. As explained, radiative feedback, setting the minimum mass of the star-forming haloes in the ionized regions, is implemented in our formalism. We shall discuss its effects in detail.

This fiducial model, which seems to fit most of the observations, is shown in Fig. 1 (see Table 1 for the values of all the parameters). It also allows us to build a self-consistent reionization scenario, whose different predictions are compared to the available data in each of the 12 panels composing the figure.

The reionization history is well exemplified by the evolution of the filling factor of ionized regions Q_i (panel b). According to the curves shown, hydrogen reionization must have taken place at redshift $z \approx 15$ while the He II reionization is completed around $z \approx 12$. We stress here that, when Q_i becomes unity, the regions having densities less than Δ_i are completely ionized thus signifying the completion of reionization, while regions with higher densities are completely neutral. Also note that $Q_{\text{HII}} \geq Q_{\text{HeIII}}$, thus showing that the He III ionization front never overtakes the H II front. Interestingly, the evolution of Q_{HeIII} is markedly affected by the hydrogen reionization; there is a decrease in Q_{HeIII} when Q_{HII} becomes unity. The reason for this is that, as more and more regions get ionized, the feedback effect depresses PopIII star formation, thus decreasing ionization rates. However, while this decrease is marginal with respect to the wealth of hydrogen ionizing photons, it profoundly affects the emissivity of photons above 54.4 eV. A more remarkable difference in the evolution of the filling factor Q_{HeIII} is however seen at redshifts $3.5 < z < 7$. During this epoch, the model predicts He III recombination followed by a second He II reionization occurring at $z \approx 3.5$; Q_{HeIII} drops to a minimum value of 0.4, i.e. He is primarily in the singly ionized state at $z \approx 5-6$.

This behaviour can be understood from panels (i)–(j), where the ionizing rates of the sources responsible for H and He ionization are shown. From these panels, we see that at high redshifts (> 10), the ionizing flux is totally dominated by PopIII stars, which however fade off at lower redshifts. PopIII stars have a hard spectrum, as seen by comparing the values of H and He ionizing rates at high redshifts in panels (i) and (j), respectively. It then follows that the PopIII stars can ionize He II quite efficiently. Once their formation is quenched, there is little source of He II ionizing photons until the QSOs take over the production of photons above 54.4 eV around redshifts of 5 (see panel j). Hence, while the first ionization of He II is controlled by PopIII stars, the second one is induced by QSO radiation. The transition epoch has been fixed in the fiducial model to $z_{\text{trans}} = 10$ and its effect on the rates can be clearly appreciated; also note that transition from PopIII to PopII stars is not instantaneous. Similar conclusions can be drawn by inspecting the star formation history in panel (h): PopIII stars produce a first maximum in the star-forming activity at $z \approx 15$ where $\dot{\rho}_{\text{SF}} \approx 0.003 M_{\odot} \text{ yr}^{-1} \text{ Mpc}^{-3}$, followed by a drop because of radiative feedback from ionized regions and a subsequent rise due to the increasing contribution of PopII stars leading to a less pronounced peak, $\dot{\rho}_{\text{SF}} \approx 0.1 M_{\odot} \text{ yr}^{-1} \text{ Mpc}^{-3}$ at $z = 4$. According to these results, only 0.3 per cent of the stars produced by $z = 2$ need to be PopIII stars in order to achieve the first reionization.

Reionization proceeds from regions of low density to overdense ones, as shown by the evolution of the critical density Δ_i for the H II and He III regions in panel (a). We recall that regions having densities above Δ_i are neutral, while a fraction Q_i of the regions with densities lower than Δ_i are ionized. By $z = 5$, ionization fronts have been able to penetrate inside quite dense regions, with $\Delta > 10^3$, leaving therefore tiny islands of neutral gas (mostly in the vicinity or part of galaxies) in a sea of ionized plasma. As the H II ionization front always leads the He III front, it is obvious that the value of Δ_{HII} is always higher than Δ_{HeIII} . Note that Δ_i is constant as long as $Q_i < 1$. Panel (c), illustrating the evolution of the clumping factor $R(\Delta_i)$ of the ionized regions, points towards the same behaviour. Its evolution is essentially determined by the lognormal distribution, being essentially constant in the pre-overlap stage where Δ_i is constant. The corresponding evolution of the mean free path $\lambda_i(z)$ for H- and He II-ionizing photons is shown in panel (e).

The derived scenario can now be directly compared with a set of different experimental constraints. We have already mentioned that the value of $\epsilon_{\text{SF,PopII}}$ is chosen such that the predicted SFR agrees with observations. However, it is still interesting to note from panel (h) that our model reproduces the observed evolution of the SFR. We next consider the number of Lyman-limit systems per unit redshift range (panel d), as computed from the mean free path for the hydrogen ionizing photons. The data points with error bars are taken from Storrie-Lombardi et al. (1994). Another useful comparison involves the mean Ly α transmitted flux, or, the effective (Gunn–Peterson) optical depth (panel k), defined as $-\ln F$, where F is the mean transmitted flux. The three curves, from right to left are for $\gamma = 1.0, 1.7, 2.4$, respectively. Although the general rising trend shown by the data (Songaila 2004) is reproduced quite well by the model, there is some indication that γ may vary, not unexpectedly, with redshift. In fact, a better agreement with the data is found if the adiabatic index increases from $\gamma = 1$ (isothermal EOS) at $z \approx 3$ to 2.4 at $z = 6$. This behaviour is opposite to simple expectations based on the assumption that reionization takes place at $z \approx 6$. Although it is true that at reionization the gas tends to approach isothermality, afterwards evolving to a higher more adiabatic state, we have to keep in mind that our fiducial model predicts that hydrogen reionization has occurred long before $z = 6$ and therefore it is physically plausible that at later evolutionary stages the EOS deviated from $\gamma = 1$; this value is eventually recovered when He II reionization occurs at $z = 3.5$.

As an additional test of the model, we next consider the IGM temperature. In particular, panel (f) shows the estimates of the mass-averaged temperature for H II and He III regions and the global one (we recall that this quantity is obtained by weighted averages over different regions, according to the mass fraction of the corresponding region). Note that this quantity continues to increase with decreasing z at lower redshifts (post-overlap stage) due to the fact that the mass-averaged temperature is dominated by regions of higher densities, and as such higher density regions get ionized gradually, the mass-averaged temperature rises. As already mentioned, the quantity usually derived from QSO absorption line experiments is the temperature at the mean density, T_0 (panel g). Because T_0 represents the thermodynamic state of the medium at mean density, its behaviour is markedly different from that of the mass-averaged temperature, particularly in the post-overlap era. As we mentioned before, the mass-averaged temperature rises because regions of higher densities get ionized, while the ionization of such regions does not affect T_0 at all. Following the first reionization, T_0 is boosted to 1.5×10^4 K; from there it decreases because of adiabatic expansion; however, the overall trend is relatively flat. A more pronounced

Table 1. Parameter values used in different figures throughout the paper.

Fig.	$\epsilon_{\text{SF,PopII}}$	$f_{\text{esc,PopII}}$	$\epsilon_{\text{SF,PopIII}}$	$f_{\text{esc,PopIII}}$	z_{trans}	v_c
1	0.1	0.005	0.007	0.9	10.0	Using equation (14)
2	0.1	0.0005	0.007	0.9	10.0	Using equation (14)
3	0.1	0.1	0.007	0.9	10.0	Using equation (14)
4	0.1	0.005	0.002	0.9	10.0	Using equation (14)
5	0.1	0.005	0.007	0.9	11.4	Using equation (14)
6	0.1	0.005	0.007	0.9	10.0	50 km s ⁻¹

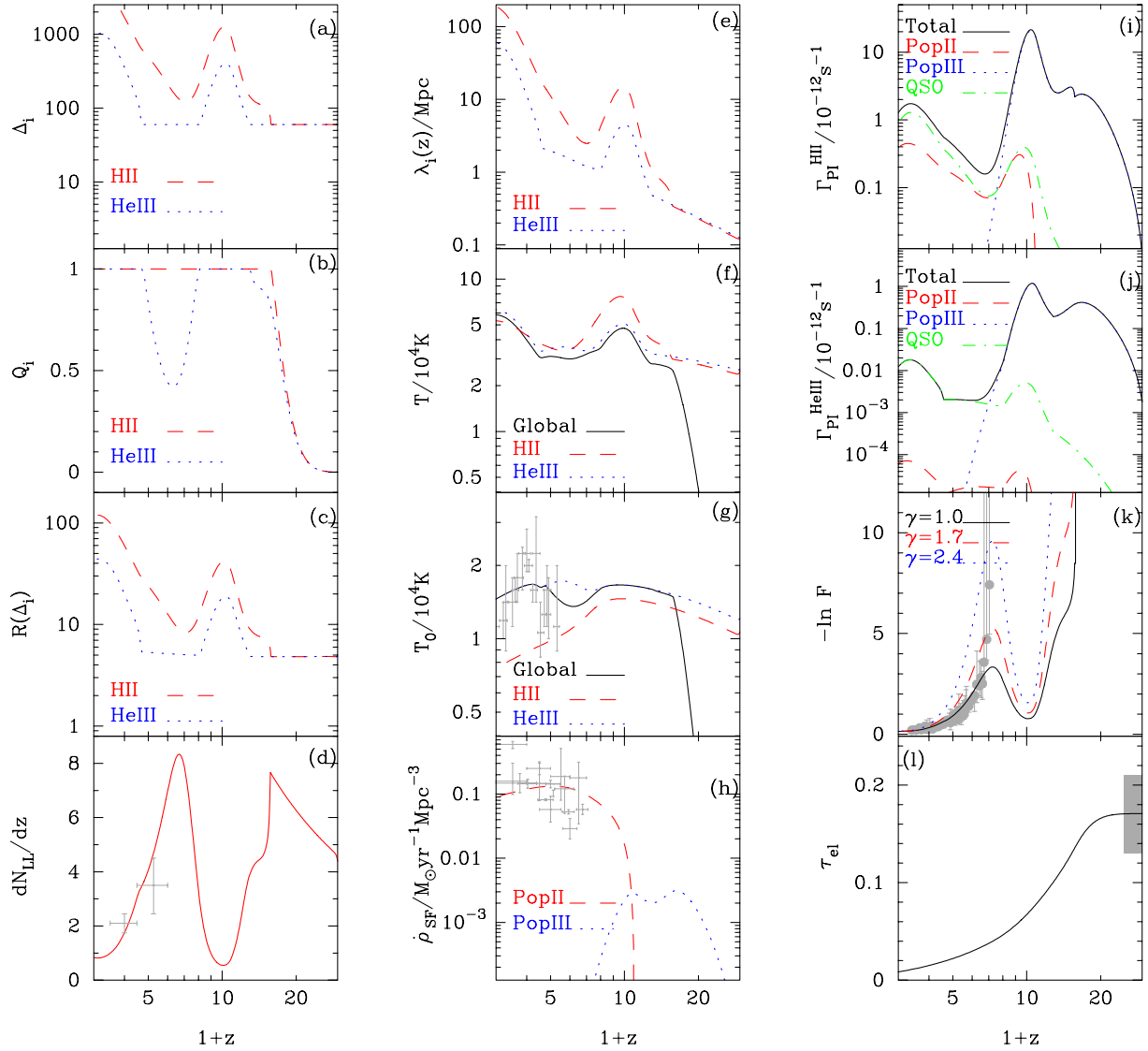


Figure 1. The fiducial model that matches all available observations. Adopted parameters are $\epsilon_{\text{PopIII}} = 7 \times 10^{-3}$, $\epsilon_{\text{PopII}} = 5 \times 10^{-4}$, $z_{\text{trans}} = 10$. The panels show as a function of redshift: (a) critical overdensity for reionization, (b) filling factor of ionized regions, (c) effective clumping factor, (d) specific number of Lyman-limit systems, (e) ionizing photons mean free path, (f) mass-weighted temperature, (g) mean-density gas temperature, (h) cosmic star formation history, (i) photoionization rates for hydrogen, (j) photoionization rates for helium, (k) Gunn–Peterson optical depth, (l) electron scattering optical depth. See text for detailed description of different panels, and Table 1 for values of all the parameters.

decrease is prevented by the newly available He II atoms from recombination of this species, which provides extra photoheating to the gas. The curve seems to fit reasonably well the data (taken from Schaye et al. 2000), although a few of them are more than 1σ away. Apparently, our model would better reproduce the exper-

imental trend if the second He II reionization could be delayed by roughly 0.5 redshift units. However, note that the data are consistent with the fact that He is singly ionized (H II regions) at $z \gtrsim 3.5$, while it is consistent with He being doubly ionized (He III regions) at $z \lesssim 3.5$. Unlike the data points, the global temperature in our models

rises gradually rather than showing a sudden jump. This is related to the fact that $Q_{\text{He III}}$ has a rather gradual rise. It might be possible that the data show a sudden jump in T_0 because it is based on a small number of lines of sight. Because we expect that there will be large fluctuations in the temperature along various lines of sight when $Q_i < 1$, one thus has to compute the temperature along numerous lines of sight to get the global mean, which can then be compared with the model. On the other hand, our model can be used to generate different lines of sight with different conditions and can be compared with existing observations. In this regard, we should mention that there are other analyses of the same data (Ricotti, Gnedin & Shull 2000) that do not show the above mentioned sudden jump in T_0 around $z \approx 3.5$ mainly because of larger error bars. In this sense, one requires much robust analysis of the observational data for more concrete conclusions. Finally, we turn in panel (l) to the electron scattering optical depth, τ_{el} . The grey shaded region is the 1σ limit as obtained from the first-year *WMAP* data. The predicted values match quite well with the *WMAP* constraint.

We conclude that our fiducial model can explain in a self-consistent manner and simultaneously all the available data existing on cosmic reionization, showing also a strong predictive power, in spite of its simple and somewhat idealized implementation. The emerging picture is one in which the universe has been initially reionized by massive PopIII stars both in H and He; the subsequent disappearance of such exotic stars, required by the NIRB, caused He III recombination, followed by its second reionization induced by QSOs. This evolution has produced little effect on hydrogen, which remained essentially ionized throughout, as its ionization state was maintained by normal PopII stars.

In the following sections, we investigate different flavours of such pictures produced by variation of the free unknown model parameters.

7.1 Constraints on the PopII ionizing efficiency

The efficiency parameter ϵ_{PopII} for the low-redshift, normal stars is one of the most ill-determined parameters of our model. We reiterate that we have, mainly for simplicity, assumed the parameter to be independent of z and galaxy mass, although there are hints from the analysis of the Sloan Digital Sky Survey data that star formation efficiency might vary with the halo mass as $M^{2/3}$ for galactic stellar masses $< 3 \times 10^{10} M_{\odot}$ (Kauffmann et al. 2004).

As discussed earlier, ϵ_{PopII} is the product of the star-forming efficiency $\epsilon_{\text{SF,PopII}}$ and the escape fraction $f_{\text{esc,PopII}}$ of photons from the halo, both of which may vary with redshift and galactic mass. The first quantity $\epsilon_{\text{SF,PopII}}$ can be reasonably constrained by comparing the model with observations of the SFR at lower redshifts. In most cases, it is found to be ≈ 10 per cent. The largest uncertainty comes from the escape fraction $f_{\text{esc,PopII}}$. It is quite difficult to determine it observationally and the current limits from different kinds of modelling vary from a few per cent to about 50 per cent.

In the fiducial model explored so far, we adopted as an educated guess $\epsilon_{\text{PopII}} = 0.05$ per cent while Fig. 2 was devised with the aim of determining a lower limit on ϵ_{PopII} from our models. However, one can realize from there that such determination is quite difficult to make from low ($z < 6$) redshift observations. The reason is that, once ϵ_{PopII} is decreased (in this case by 10 times with respect to the fiducial one), PopII stars play a subdominant role and observations can be explained just with the ionizing photons from PopIII stars and QSOs. This does not necessarily mean that the contribution from the PopII stars is insignificant or unnecessary, but it is just that the present observations have very little dependence on PopII star

efficiency once below a certain threshold. We believe lower limits on ϵ_{PopII} should be derived from some other considerations.

On the other hand, it is possible to obtain a stringent upper limit on ϵ_{PopII} , as shown by Fig. 3. In fact, if $\epsilon_{\text{PopII}} > 0.01$, then the number of ionizing photons produced will be too high, yielding a too low Ly α optical depth (or equivalently, a higher transmitted flux) than the observed value at redshifts around ~ 3 . Note that, for a star-forming efficiency of 10 per cent, this upper limit corresponds to an escape fraction of 10 per cent, which should be considered as quite stringent. Also to be noted is that the temperature of the He III regions is lower than that observed around $z \approx 3.5$, hence this higher value of ϵ_{PopII} is unable to match the high T_0 at those redshifts. The reason for this is that with such a high production of photons from PopII stars, the ionizing spectrum is no more dominated by QSOs and thus effectively becomes much softer. This, in turn, results in lower values of T_0 for He III regions.

There is one more point that needs to be clarified in this section. We have noted that the change in the value of ϵ_{PopII} affects the low-redshift physics only. On the other hand, one can see by comparing panels (i) and (j) of Figs 1, 2 and 3 that the values of Γ_{PI} are lower at high redshifts when we increase ϵ_{PopII} . This apparent contradiction arises from the fact the value of the photon mean free path λ_0 in equation (39) is chosen so as to match the low-redshift observations. When ϵ_{PopII} is increased, the number of photons is higher, leading to potentially larger ionized regions. In order to control the size of the regions so that they match low-redshift observations, we have to decrease the value of λ_0 . In turn, this decreases the ionization (and heating) rates at higher redshifts.

7.2 Constraints on the PopIII ionizing efficiency

As in the previous section, let us now try to determine the limits on ϵ_{PopIII} (without changing the value of z_{trans}). In contrast to the case for ϵ_{PopII} , the major uncertainty in ϵ_{PopIII} comes from the star-forming efficiency $\epsilon_{\text{SF,PopIII}}$. The escape fraction at such high redshifts is usually quite high (nearly 100 per cent) for low-mass haloes because typically only a few PopIII stars are required to completely ionize the parent galaxy (the masses of PopIII-hosting galaxies are low). However, our understanding of the star formation process and constraints of parameters at high redshifts are quite limited because of the unavailability of direct observations. For the moment, the best constraints on $\epsilon_{\text{SF,PopIII}}$ come from the NIRB.

Because ϵ_{PopIII} does not affect the low-redshift observations, the most stringent limits on it come from the constraints on τ_{el} . In fact, matching the *WMAP* constraint requires that this efficiency is confined in the range $0.002 < \epsilon_{\text{PopIII}} < 0.03$. We would like to stress that, for the assumed value of z_{trans} , this constraint on ϵ_{PopIII} is independent of the constraints obtained from the NIRB data. The lower limit on ϵ_{PopIII} implies that, in order to match the *WMAP* constraints, one requires a star-forming efficiency of $\epsilon_{\text{SF,PopIII}} = 0.2$ per cent if $f_{\text{esc}} = 1$ (probably reasonable for low-mass haloes), while in case the escape fraction is much lower, say, $f_{\text{esc}} = 10$ per cent (probably true for high-mass haloes), then one needs a star-forming efficiency as high as 2 per cent. Also note that the above limits are obtained for a transition redshift of $z_{\text{trans}} = 10$. The value of z_{trans} is quite well constrained to be $\gtrsim 9$ from NIRB studies. However, for the sake of completeness, we would like to discuss the dependence of these limits on z_{trans} . For higher (lower) values of ϵ_{PopIII} , one has to take higher (lower) values of z_{trans} to obtain the same value of τ_{el} . Physically, this implies that one can either let the PopIII stars form efficiently but survive for a shorter time, or let them form inefficiently but survive longer, so that the number of

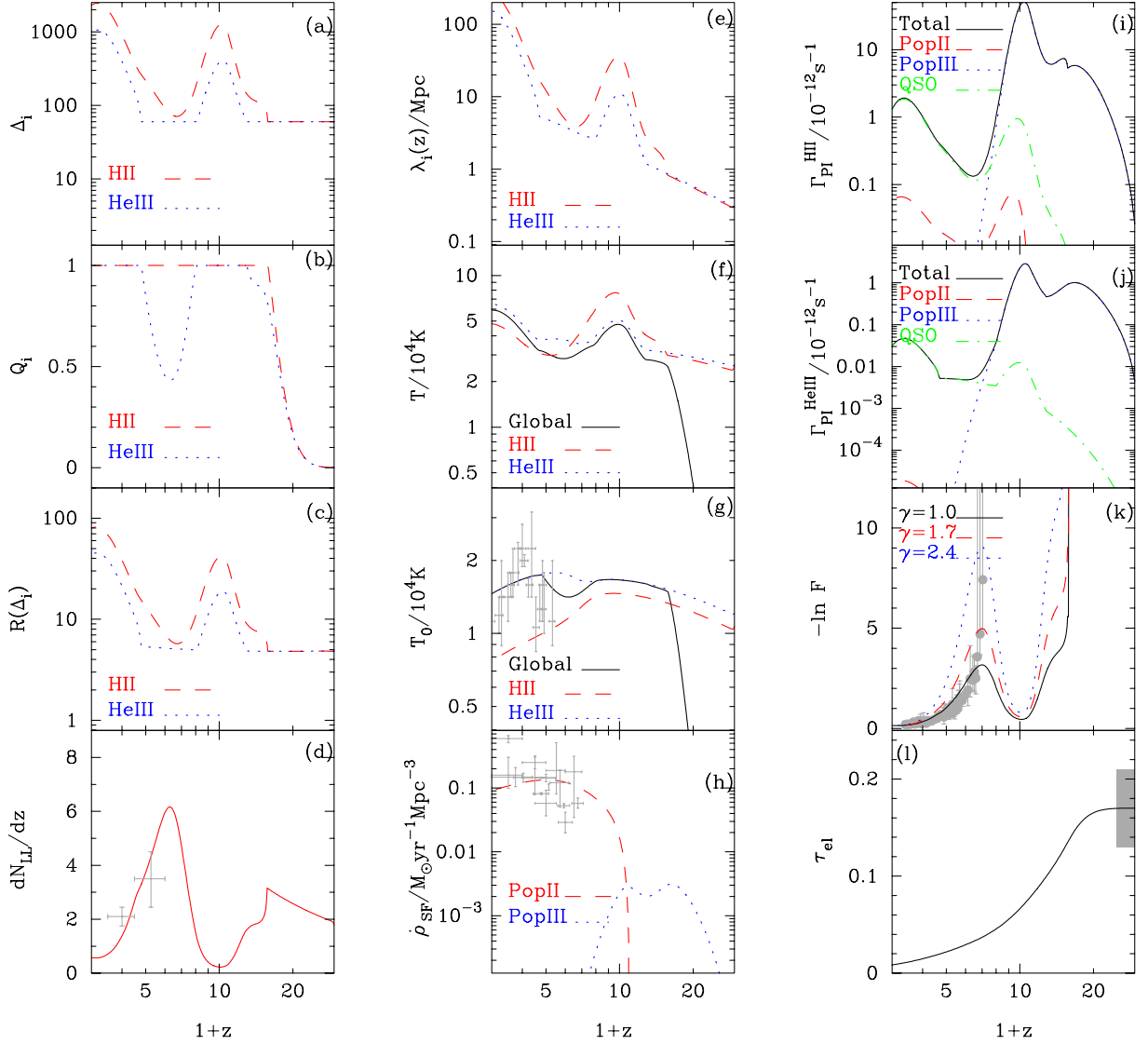


Figure 2. Same as in Fig. 1, but for $\epsilon_{\text{PopII}} = 5 \times 10^{-5}$. See Table 1 for values of all the parameters.

free electrons produced is similar. As noted from NIRB studies, the value of z_{trans} we are using is somewhat a lower limit. This implies that the lower limit of 0.002 on ϵ_{PopIII} (the case illustrated in Fig. 4) is quite solid. On the other hand, one can allow for values larger than 0.02 if the value of z_{trans} is allowed to be larger. Thus, given the present observational constraints, it is slightly difficult to put a tight upper limit on ϵ_{PopIII} with uncertainties in z_{trans} . On the other hand, if we fix the value of z_{trans} from NIRB (or other studies in the future), our model can constrain the value of ϵ_{PopIII} quite stringently.

7.3 Reionization constraints

In this section, we study the constraints on the reionization of both hydrogen and He II with respect to the uncertainties in various free parameters of the fiducial model. We have seen that the fiducial model predicts that He II was first completely reionized at $z \approx 12$. However, it turns out that the values of z_{trans} and ϵ_{PopIII} can affect the He II reionization at such high redshifts. Because He II reionization is not complete before $z \approx 12$, it is obvious that a value of $z_{\text{trans}} > 12$ will prohibit a complete reionization of He II. However, as is seen

from NIRB studies, it is most likely that the value of z_{trans} may not be much larger than 10. On the other hand, for smaller values of ϵ_{PopIII} , it is possible that there are not enough photons from PopIII stars and the He II reionization at high redshifts is not complete. However, in the extreme case where $\epsilon_{\text{PopIII}} = 0.002$ (the lowest allowed value from *WMAP* constraints), we find that Q_{HeIII} achieves a maximum value of unity around $z \approx 10$ (see Fig. 4). This implies that He II must be completely reionized at high redshifts as long as the value of ϵ_{PopIII} does not violate the *WMAP* constraint.

Although our fiducial model predicts He II recombination after its first reionization followed by a second reionization driven by QSOs ionizing power, a similar double reionization of H does not appear to have occurred according to our analysis. The physical interpretation of He II recombination at $3.5 < z < 7$ is found in the rather abrupt halt in the PopIII star formation activity at $z \approx 9$; as a consequence, the total number of He II-ionizing photons drops considerably and the second He II reionization has to wait for the newly available ones produced by QSOs. This scenario seems to strongly imply a double He II reionization (keeping in mind that the first reionization might not be complete for lower values of

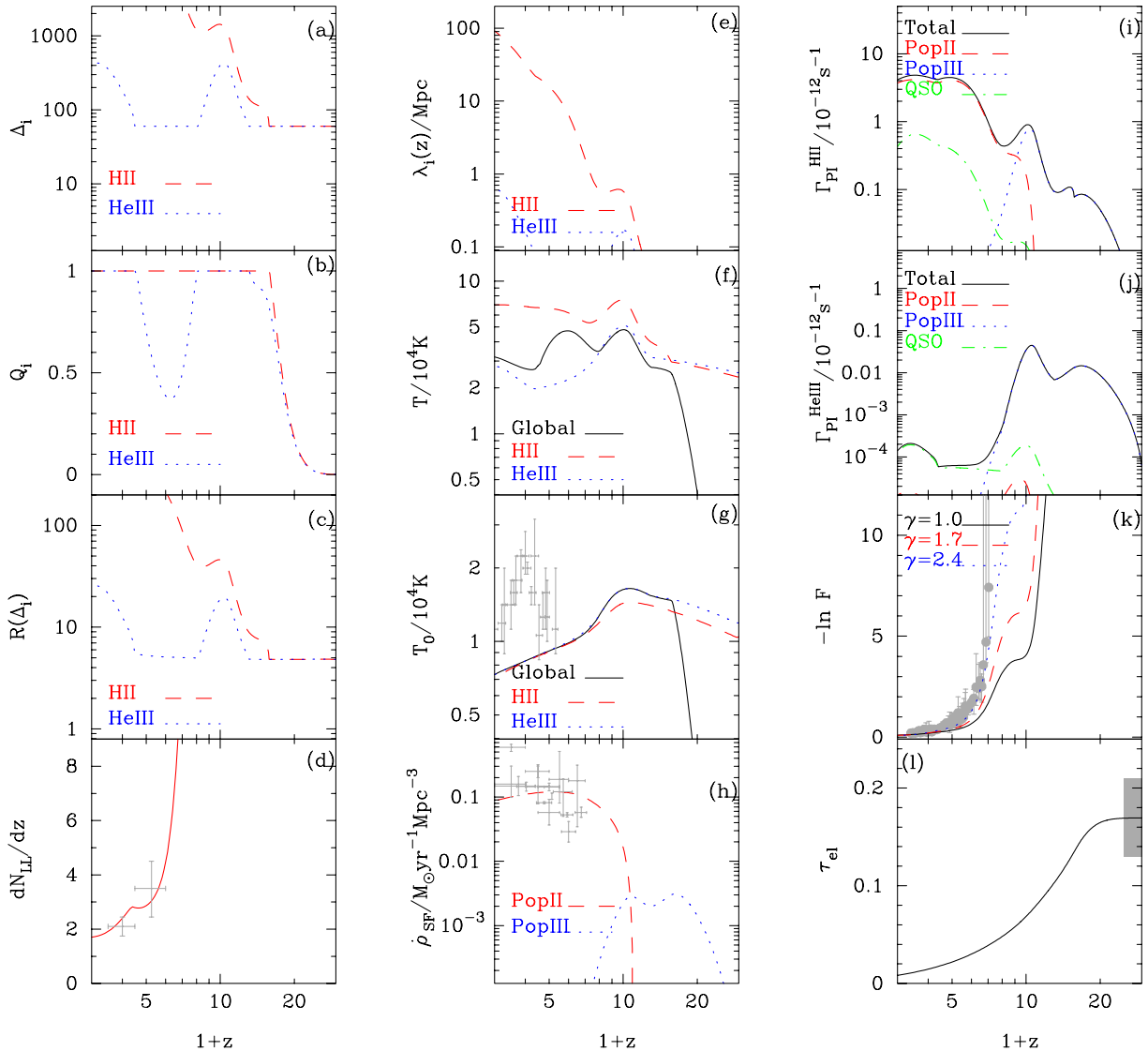


Figure 3. Same as in Fig. 1, but for $\epsilon_{\text{PopII}} = 0.01$. See Table 1 for values of all the parameters.

ϵ_{PopIII} or for higher values of z_{trans}). Hydrogen, however, behaves differently due to the larger availability of photons with energies above 13.6 eV, which are produced also by galaxies in addition to QSOs. Hence the photoionization rate of H remains high enough to keep H atoms in the ionized state. A double H reionization could only occur if the time gap between the turn-on of PopIII stars and the rise of PopII ones is increased, i.e. if a larger z_{trans} value is assumed. This case has been explored and is shown in Fig. 5, where we have fixed $z_{\text{trans}} = 11.4$. Such model predicts a double H reionization around $z = 8$, but it is at odds with the constraints from the NIRB, which require PopIII stars down to redshift of about 9 in order to fit the background intensity (and fluctuations) observed in the *J* band (Salvaterra & Ferrara 2003; Magliocchetti et al. 2003). This scenario is a vanilla one for future IGM detection via the H I 21-cm line, as the redshifted emission could be observed in the best range of frequencies and sensitivities of radio telescopes like the Low Frequency Array³ (Ciardi & Madau 2003; Iliev et al. 2002).

³ <http://www.lofar.org>

7.4 Different radiative feedback models

In this section, we analyse the effects of varying the strength of the radiative feedback we have imposed on the reionization process. As we have already noted, the radiative feedback affects the He II reionization as well as SFR at high redshifts. Hence it is important to check how the results vary once we change our assumptions regarding the feedback mechanism. In our fiducial model, we have taken the minimum circular velocity of star-forming haloes in the ionized regions to be evolving depending on the temperature of the region (see equation 14). However, a different feedback prescription is to fix the minimum circular velocity of haloes allowed to form stars at a given value, which we take to be $v_c = 35 \text{ km s}^{-1}$, following (Gnedin 2000; Kitayama et al. 2001).

We have first explored such a case. However, a comparison with the fiducial model, has shown hardly any significant differences. Therefore we have further increased v_c to 50 km s^{-1} (a value at the upper limit of the physically admissible range derived by the above mentioned studies). The corresponding result is shown in Fig. 6. While most of the results are unaffected, we find that the

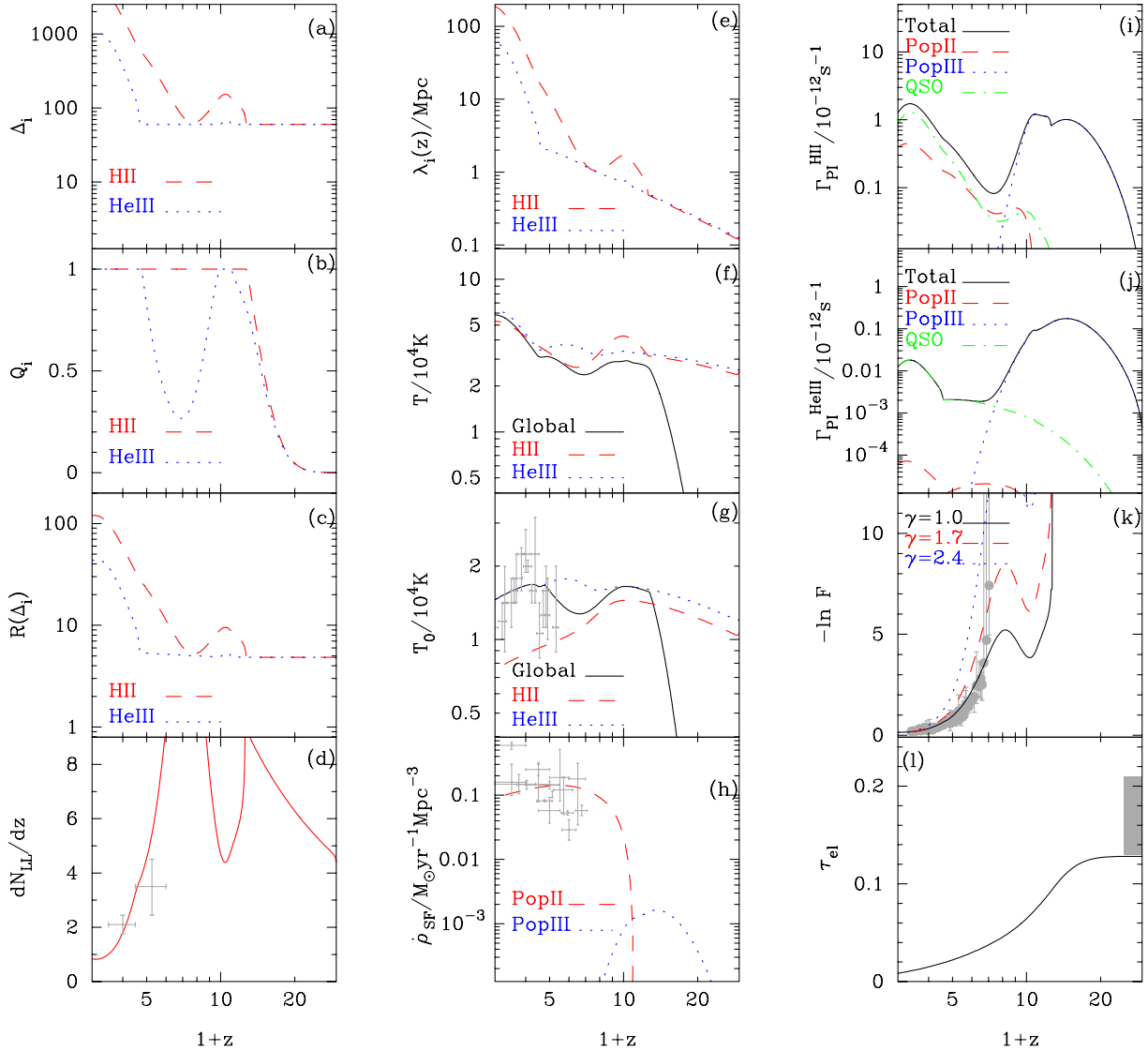


Figure 4. Same as in Fig. 1, but for $\epsilon_{\text{PopIII}} = 0.002$. See Table 1 for values of all the parameters.

strong radiative feedback suppresses the growth of He III regions and delays the (first) reionization of He II. As one can see from panel (b), there is substantial decrease in Q_{HeIII} when Q_{HII} becomes unity, thus delaying the He II reionization until $z \approx 10$. Even this extreme case, however, does not change the qualitative evolution of reionization with respect to the standard one adopted in all other cases. Whether this strong radiative feedback has any observational consequence is not clear as all the other considered quantities are essentially unaffected by the choice of minimum circular velocity.

7.5 Reduced power on smaller scales

Finally, we briefly mention some of the other physical processes that could reduce the power of density fluctuations on smaller scales and hence influence our results. The first such process is the suppression of cooling in minihaloes (i.e. haloes having virial temperatures less than 10^4 K) due to photodissociation of molecular hydrogen. It is also possible that the minihaloes do not contribute to reionization due to confinement of H II regions from feedback effects (Ricotti, Gnedin & Shull 2002). This would increase effectively the value

of $M_{\text{min}}(z)$ used in equation (8). Because these minihaloes can potentially contribute a substantial number of ionizing photons from PopIII stars at high redshifts, it is obvious that one has to use a relatively higher value of ϵ_{PopIII} in the case when the minihaloes are not forming stars so as to match the *WMAP* constraints. It turns out that one requires $\epsilon_{\text{PopIII}} > 0.007$ to match the *WMAP* limits. This implies that if the high-mass haloes have an escape fraction $f_{\text{esc}} = 10$ per cent, then the required value of star-forming efficiency would be as high as 7 per cent, while lower values of the escape fraction would require higher star-forming efficiencies. Once such a higher value of ϵ_{PopIII} is chosen, we found that there is hardly any difference in the reionization history of hydrogen when compared to the fiducial model. The reionization of He II at high redshifts, however, occurs much earlier because of less severe feedback from ionized H II regions; in fact, He II reionizes almost simultaneously with hydrogen. To understand this, note that the effect of feedback is to suppress the photon production in low-mass haloes (which were capable of producing photons before the medium was heated up) in the ionized (and heated) regions: hence, it should be obvious that the feedback is more severe when there are more low-mass haloes

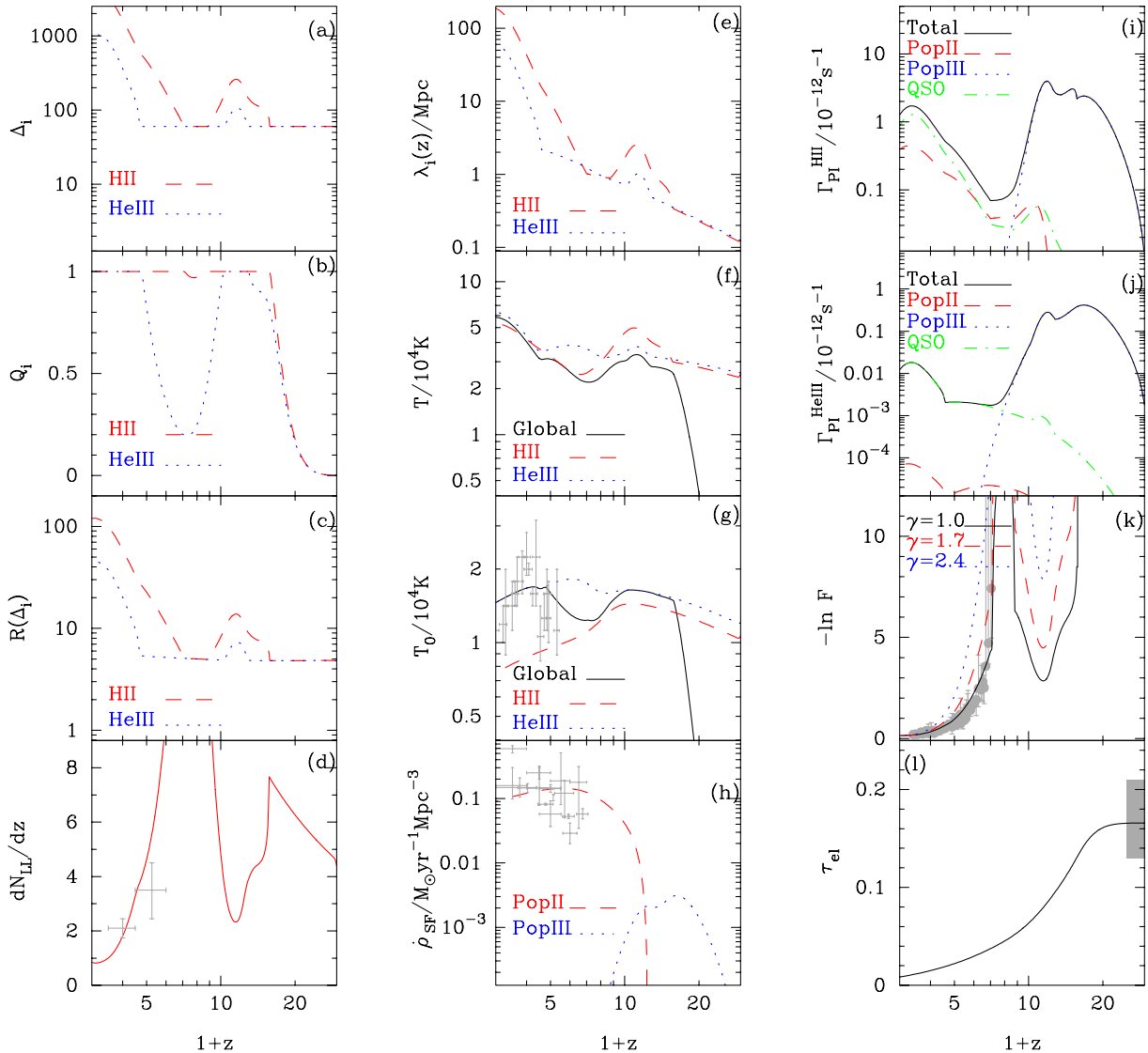


Figure 5. Same as in Fig. 1, but for $z_{\text{trans}} = 11.4$. See Table 1 for values of all the parameters.

forming stars. It is precisely because of this reason that the feedback plays a relatively subdominant role when the number of low-mass star-forming haloes is reduced. Feedback effects are instead more severe in our fiducial model, where the low-mass haloes are allowed to form stars efficiently. Interestingly, a similar effect is produced by smaller values of the fluctuation spectrum index n , as a result of the reduced small-scale power.

8 SUMMARY AND CONCLUSIONS

We have developed a simple formalism to study cosmic reionization and the thermal history of the IGM. In spite of its simplicity, the formalism implements most of the relevant physics governing these processes in a self-consistent manner, including the inhomogeneous IGM density distribution, three different classes of ionizing photon sources (massive PopIII stars, PopII stars and QSOs), and radiative feedback inhibiting the formation of stars in galaxies below a certain circular velocity threshold. Such approach allows us to predict the star formation/emissivity history of the source, follow the evolution of H and He reionization and of the intergalactic gas temperature,

along with a number of additional predictions involving directly observable quantities.

By comparing these results with the available experimental data, we have selected a ‘fiducial’ model. This fiducial model self-consistently predicts values matching very well all the available observational data, i.e. the redshift evolution of Lyman-limit absorption systems, Gunn–Peterson and electron scattering optical depths, and the cosmic star formation history without the need to further adjust the free parameters, which are essentially the efficiencies of ionizing photon production for PopIII and PopII stars denoted by ϵ_{PopIII} and ϵ_{PopII} , respectively. In principle, a third parameter, z_{trans} , the epoch of cosmic transition from PopIII to PopII stars enters the calculations, but in practice this values is bound to values very close to $z \approx 9$ by the analysis of the NIRB data.

The emerging scenario from our analysis can be summarized in a few points, which follow.

(i) Hydrogen reionization must have taken place at $z \approx 15$, while He II must have been reionized by $z \approx 12$, taking into account the maximum uncertainty in the value of ϵ_{PopIII} (we recall that the

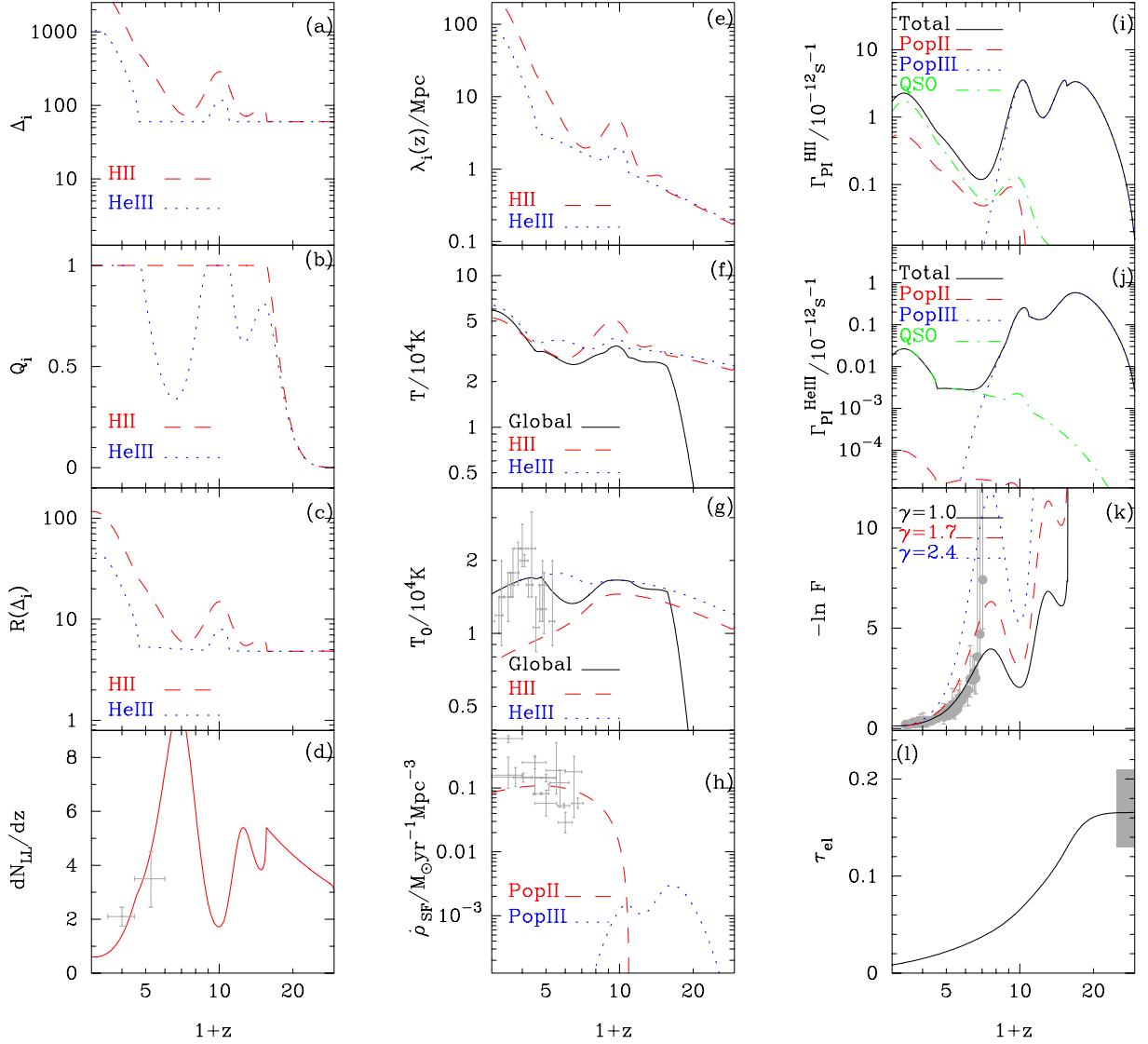


Figure 6. Same as in Fig. 1, but for a fixed minimum circular velocity of star-forming haloes $v_c = 50 \text{ km s}^{-1}$. See Table 1 for values of all the parameters.

ionizing photon efficiency is defined as the product of the star formation efficiency and the escape fraction, $\epsilon \equiv \epsilon_{\text{SF}} f_{\text{esc}}$ for each population). At about $z = 7$, He III suffered an almost complete recombination ($Q_{\text{He III}} \approx 0.4$) as a result of the extinction of PopIII stars (the only contributors of photons with energies above 54.4 eV at that redshift), an occurrence required by the interpretation of the NIRB. A complete reionization of He III occurs at $z = 3.5$ and it is driven by hard photons produced by QSOs. Double H reionization does not take place due to the larger availability of photons above 13.6 eV from PopII stars in galaxies and from QSOs, even after all PopIII stars disappear.

(ii) Following the first reionization, the temperature of the IGM corresponding to the mean gas density, T_0 , is boosted to $1.5 \times 10^4 \text{ K}$; from there it decreases because of adiabatic expansion; however, the overall trend is relatively flat. Observations are consistent with the predicted temperature of the H II regions at $z \gtrsim 3.5$, while they are consistent with the temperature of the He III regions at $z \lesssim 3.5$. This could be interpreted as a signature for the (second) reionization of He II; however, the global (mass-averaged) temperature rises gradually rather than showing a sudden jump. This alleged jump in the

data (Schaye et al. 2000) might be a spurious feature induced by fluctuations along the limited number of lines of sight used by the absorption line experiments, or it is possible that the jump does not have a strong enough statistical significance (e.g. see the analysis by Ricotti et al. 2000).

(iii) PopIII stars produce a first maximum in the star-forming activity at $z \approx 15$ where $\dot{\rho}_{\text{SF}} \approx 0.003 \text{ M}_{\odot} \text{ yr}^{-1} \text{ Mpc}^{-3}$, followed by a drop and a subsequent rise due to the increasing contribution of PopII stars leading to a less pronounced peak, $\dot{\rho}_{\text{SF}} \approx 0.1 \text{ M}_{\odot} \text{ yr}^{-1} \text{ Mpc}^{-3}$ at $z = 4$. These results also suggest that only a 0.3 per cent of the stars produced by $z = 2$ need to be PopIII stars in order to achieve the first reionization. We point out that the fiducial model not only correctly predicts at the same time the IGM reionization and thermal history but it reproduces (with the same free parameters) the cosmic star formation history data at $z < 6$.

In addition to the above features, the data yield the following constraints on these free parameters: $\epsilon_{\text{PopII}} < 0.01$, $0.002 < \epsilon_{\text{PopIII}} < 0.03$. Varying the efficiencies in these two ranges does not affect most of the general scenario emerging from the first two points

above. We have experimented with maximally strong radiative feedback finding that the only difference with respect to the fiducial case is to suppress the growth of He III regions at $z > 10$ and thus delay the reionization of He II. Feedback effects impact the ionization history of He II less severely when the minihaloes (i.e. haloes with virial temperature $T_{\text{vir}} < 10^4$ K) at high redshifts are not able to cool and form stars, or when the index of the density power spectrum is smaller. However, when the contribution from the minihaloes is ignored, one requires a higher value of star-forming efficiency to match the *WMAP* constraints.

Before concluding, we critically discuss our results in the light of previous numerical works and semi-analytical arguments in the literature. A few full numerical simulations of cosmic reionization including radiative transfer have been performed after the *WMAP* results (Ciardi, Ferrara & White 2003; Sokasian et al. 2003; Gnedin 2004; Ricotti & Ostriker 2004a; Sokasian et al. 2004). These works use a very different set of assumptions concerning the IMF of the first stars, feedback effects and recipes for the subgrid physics and radiative transfer schemes. Therefore, a detailed comparison is not possible for all these works. Ciardi et al. (2003) concentrated on reproducing the *WMAP* Thomson optical depth in a reionization model dominated by ‘normal’ (i.e. not very massive) PopIII stars forming in objects with $T_{\text{vir}} > 10^4$ K: minihaloes are thus suppressed (according to our results this should not make a sensible difference) but no radiative feedback is included for objects just above this threshold. This results in an SFR nearly 10 times larger than we predict for $z > 10$. Because of the compensating effects of the IMF and star formation history, hydrogen reionization is achieved at about the same redshift (14.7) as in our case. It is not clear if this model is able to explain the Gunn–Peterson opacity as the simulation ends at $z \approx 8$. Gnedin (2004) took the opposite approach to the problem, focussing on the fit to the Ly α mean transmitted flux. The value of ϵ_{SF} is fixed by normalizing the SFR to its observed value at $z = 4$ and, therefore, as we also satisfy this constraint, it should be similar to the one adopted here. The production of ionizing photons (which includes our choice of the IMF and of the escape fraction) is set by construction to the value allowing the best fit to the transmitted flux. Hydrogen reionization occurs at $z = 6.1 \pm 0.3$ in the fiducial model of Gnedin (2004), which corresponds to $\tau_{\text{el}} = 0.06$: quite outside the canonical *WMAP* value $\tau_{\text{el}} = 0.17 \pm 0.04$. Although the quoted error is somewhat uncertain,⁴ such a low value for τ_{el} seems to be very unlikely. For this reason Gnedin suggests that the reionization history prior to the hydrogen reionization must have been much more complex than the smooth, monotonic behaviour obtained from his simulations. Our results do not require such a complex history. The observed Gunn–Peterson optical depth rise towards $z = 6$ is simply caused by the drop of the photoionization rate (see panel i of Fig. 1) following the disappearance of PopIII stars, thus causing a significant increase of the hydrogen neutral fraction. To be more

quantitative, we find that the mass-averaged neutral fraction climbs from $\approx 2 \times 10^{-4}$ at $z = 4$ to a maximum of $\approx 5 \times 10^{-4}$ at $z = 6$; following that it decreases until $z = 9$ where it reaches the value $\approx 4 \times 10^{-5}$. This behaviour closely tracks (but with opposite derivative) the evolution of the photoionization rate in the fiducial model (see panel i of Fig. 1). It is also consistent with the trend, found e.g. by Fan et al. (2002), which explains the good agreement with the Gunn–Peterson optical depth of panel (k). The actual values we find might indicate at $z \approx 6$ a slightly less neutral medium than found by Fan et al. (2002) using Ly α line: the most reliable determination is $x_{\text{HI}} > 5 \times 10^{-3}$ when mass-averaged, while $x_{\text{HI}} > 2 \times 10^{-4}$ when volume-averaged. To compare with the volume-averaged quantity, we can use our predictions corresponding to the mean density, which can be shown to yield the same answer within about 15 per cent. For the volume-averaged neutral fraction, we find a value in the range $1\text{--}2 \times 10^{-4}$, which is in good agreement with the data. Because Fan et al. (2002) state that the volume-averaged fraction should be considered as more reliable, we can consider this prediction as a success of our model.

Two more arguments that have been put forward concerning reionization history are worth discussing. The first point concerns a higher value of the lower limit (10 per cent) for the neutral fraction derived by Wyithe & Loeb (2004), based on the size of the ionizing radiation influence region around two QSOs at $z \approx 6.3$ (see also Mesinger, Haiman & Cen 2004). In brief, the argument used is that the size of the ionized region derived from observations is smaller than what expected if $x_{\text{HI}} \lesssim 10^{-3}$, as we argue above. A considerable number of uncertainties could jeopardize this conclusion: (i) the lifetime of QSOs; (ii) the effect of peculiar velocities; (iii) radiative transfer (shadowing) effects occurring in the dense environment surrounding high-redshift QSOs (iv) determination of the actual H II region size from the spectrum. For these reasons, we feel that using this argument as a constrain to reionization models is still premature.

The second point concerns the temperature evolution of the IGM. Hui & Haiman (2003), following the original proposal by Theuns et al. (2002), noted that, as long as the universe is reionized before $z = 10$ and remains highly ionized thereafter, the IGM reaches an asymptotic thermal state that is too cold compared with observations at $z = 2\text{--}4$. This indeed applies to our fiducial case, which predicts a redshift of hydrogen reionization ≈ 15 . There not only do we find that the temperature is decreasing relatively slowly due to the photoheating provided by He complex reionization history, but also that global temperature rises gradually (following the smooth $Q_{\text{He III}}$ growth) rather than showing a sudden jump. We have speculated that the observed sudden jump in T_0 (i.e. the temperature of mean density gas) might be a spurious effect due to the limited available number lines of sight. This hypothesis could be checked in the future by using our results to generate different lines of sight to be compared directly with observations. Also, it is possible that the statistical significance is much weaker, particularly if the error bars on T_0 are larger than shown here (Ricotti et al. 2000).

As a final note, it is useful to remember that our study has not included one possible additional contribution to the ionizing background due to thermal emission from gas shock heated during cosmic structure formation, recently suggested by Miniati et al. (2004). Such emission is characterized by a hard spectrum extending well beyond 54.4 eV and, according to that study, it is comparable to the QSO intensity at redshift $\gtrsim 3$. Thermal photons alone could be enough to produce and sustain He II reionization already at $z = 6$. If this prediction is correct, the partial recombination of He III seen

⁴ The uncertainty quoted for this number depends on the analysis technique employed. Fitting the temperature–polarization (TE) cross-power spectrum to Λ CDM models in which all parameters except τ_{el} assume their best-fitting values based on the temperature (TT) power spectrum, Kogut et al. (2003) obtain a 68 per cent confidence range, $0.13 < \tau_{\text{el}} < 0.21$ (the one adopted in this paper). Fitting all parameters simultaneously to the TT and the TE data, Spergel et al. (2003) obtain $0.095 < \tau_{\text{el}} < 0.24$. Including additional data external to *WMAP*, these authors were able to shrink their confidence interval to $0.11 < \tau_{\text{el}} < 0.23$. Finally, by assuming that the observed TT power spectrum is scattered to produce the observed TE cross-power spectrum, Kogut et al. (2003) infer $0.12 < \tau_{\text{el}} < 0.20$.

between redshifts 3.5 and 8 in our fiducial model might be prevented by such radiation. The present results make the test of the He state at these intermediate redshifts a crucial benchmark to assess the importance of such thermal emission.

ACKNOWLEDGMENTS

The authors would like to thank R. Salvaterra for useful discussions and the referee, M. Ricotti, for enlightening comments.

REFERENCES

- Bi H., Davidsen A. F., 1997, *ApJ*, 479, 523
 Chiu W. A., Ostriker J. P., 2000, *ApJ*, 534, 507
 Choudhury T. R., Padmanabhan T., 2002, *ApJ*, 574, 59
 Choudhury T. R., Srianand R., 2002, *MNRAS*, 336, L27
 Choudhury T. R., Srianand R., Padmanabhan T., 2001a, *ApJ*, 559, 29
 Choudhury T. R., Padmanabhan T., Srianand R., 2001b, *MNRAS*, 322, 561
 Ciardi B., Ferrara A., 2005, *Space Sci. Rev.*, 116, 625
 Ciardi B., Madau P., 2003, *ApJ*, 596, 1
 Ciardi B., Ferrara A., White S. D. M., 2003, *MNRAS*, 344, L7
 Cooray A., Bock J. J., Keatin B., Lange A. E., Matsumoto T., 2004, *ApJ*, 606, 611
 Fan X. et al., 2000, *AJ*, 120, 1167
 Fan X. et al., 2001, *AJ*, 122, 2833
 Fan X., Narayanan V. K., Strauss M. A., White R. L., Becker R. H., Pentericci L., Rix H., 2002, *AJ*, 123, 1247
 Fan X. et al., 2003, *AJ*, 125, 1649
 Fuller T. M., Couchman H. M. P., 2000, *ApJ*, 544, 6
 Gnedin N. Y., 2000, *ApJ*, 542, 535
 Gnedin N. Y., 2004, *ApJ*, 610, 9
 Haardt F., Madau P., 1996, *ApJ*, 461, 20
 Hui L., Haiman Z., 2003, *ApJ*, 596, 9
 Iliiev I. T., Shapiro P. R., Ferrara A., Martel H., 2002, *ApJ*, 572, L123
 Kashlinsky A., Arendt R., Gardner J. P., Mather J. C., Moseley S. H., 2004, *ApJ*, 608, 1
 Kauffmann G., White S. D. M., Heckman T. M., Ménard B., Brinchmann J., Charlot S., Tremonti C., Brinkmann J., 2004, *MNRAS*, 353, 713
 Kitayama T., Susa H., Umemura M., Ikeuchi S., 2001, *MNRAS*, 326, 1353
 Kitayama T., Yoshida N., Susa H., Umemura M., 2004, *ApJ*, 613, 631
 Kogut A. et al., 2003, *ApJS*, 148, 161
 Lacey C., Cole S., 1993, *MNRAS*, 262, 627
 Leitherer C. et al., 1999, *ApJS*, 123, 3
 Madau P., Haardt F., Rees M. J., 1999, *ApJ*, 514, 648
 Magliocchetti M., Salvaterra R., Ferrara A., 2003, *MNRAS*, 342, L25
 Mesinger A., Haiman Z., Cen R., 2004, *ApJ*, 613, 23
 Mahmood A., Devriendt J. E. G., Silk J., 2005, *MNRAS*, 359, 1363
 Miniati F., Ferrara A., White S. D. M., Bianchi S., 2004, *MNRAS*, 348, 964
 Miralda-Escudé J., 2003, *ApJ*, 597, 66
 Miralda-Escudé J., Cen R., Ostriker J. P., Rauch M., 1996, *ApJ*, 471, 582
 Miralda-Escudé J., Haehnelt M., Rees M. J., 2000, *ApJ*, 530, 1 (MHR)
 Nagamine K., Cen R., Hernquist L., Ostriker J. P., Springel V., 2004, *ApJ*, 610, 45
 Navarro J. F., Frenk C. S., White S. D. M., 1996, *ApJ*, 462, 563
 Petitjean P., Webb J. K., Rauch M., Carswell R. F., Lanzetta K., 1993, *MNRAS*, 262, 499
 Ricotti M., Ostriker J. P., 2004a, *MNRAS*, 350, 539
 Ricotti M., Ostriker J. P., 2004b, *MNRAS*, 352, 547
 Ricotti M., Shull J. M., 2000, *ApJ*, 542, 548
 Ricotti M., Gnedin N. Y., Shull J. M., 2000, *ApJ*, 534, 41
 Ricotti M., Gnedin N. Y., Shull J. M., 2002, *ApJ*, 575, 49
 Salvaterra R., Ferrara A., 2003, *MNRAS*, 339, 973
 Sasaki S., 1994, *PASJ*, 46, 427
 Schaerer D., 2002, *A&A*, 382, 28
 Schaye J., Theuns T., Rauch M., Efstathiou G., Sargent W. L. W., 2000, *MNRAS*, 318, 817
 Schirber M., Bullock J. S., 2003, *ApJ*, 584, 110
 Schneider R., Ferrara A., Natarajan P., Omukai K., 2002, *ApJ*, 571, 30
 Schneider R., Ferrara A., Salvaterra R., Omukai K., Bromm V., 2003, *Nat*, 422, 869
 Shapiro P. R., Giroux M. L., 1987, *ApJ*, 321, L107
 Silk J., Rees M. J., 1998, *A&A*, 331, L1
 Sokasian A., Abel T., Hernquist L., Springel V., 2003, *MNRAS*, 344, 607
 Sokasian A., Yoshida N., Abel T., Hernquist L., Springel V., 2004, *MNRAS*, 350, 47
 Songaila A., 2004, *AJ*, 127, 2598
 Spergel D. N. et al., 2003, *ApJS*, 148, 175
 Storrie-Lombardi L. J., McMahon R. G., Irwin M. J., Hazard C., 1994, *ApJ*, 427, L13
 Theuns T., Schaye J., Zaroubi S., Kim T., Tzanavaris P., Carswell B., 2002, *ApJ*, 567, L103
 Venkatesan A., Giroux M. L., Shull J. M., 2001, *ApJ*, 563, 1
 Viel M., Matarrese S., Mo H. J., Haehnelt M. G., Theuns T., 2002, *MNRAS*, 329, 848
 Whalen D., Abel T., Norman M. L., 2004, *ApJ*, 610, 14
 White R. L., Becker R. H., Fan X., Strauss M. A., 2003, *AJ*, 126, 1
 Wyithe J. S. B., Loeb A., 2003, *ApJ*, 586, 693
 Wyithe S., Loeb A., 2004, *Nat*, 427, 815

This paper has been typeset from a $\text{\TeX}/\text{\LaTeX}$ file prepared by the author.